NASA Technical Paper 3506

Damage Tolerance of Candidate Thermoset Composites for Use on Single Stage to Orbit Vehicles

A.T. Nettles, D. Lance, and A. Hodge
Marshall Space Flight Center • MSFC, Alabama

National Aeronautics and Space Administration
Marshall Space Flight Center • MSFC, Alabama 35812

September 1994

TABLE OF CONTENTS

LIST OF ILLUSTRATIONS

LIST OF ILLUSTRATIONS (Continued)

LIST OF TABLES

TECHNICAL PAPER

DAMAGE TOLERANCE OF CANDIDATE THERMOSET COMPOSITES FOR USE ON SINGLE STAGE TO ORBIT VEHICLES

I. INTRODUCTION

As NASA sets its sights on single stage to orbit (SSTO) reusable vehicles, the need for weight reduction is becoming critical. These vehicles must use advanced materials that possess a multitude of improved properties (lower density, higher stiffness and strength, resistance to damage and moisture absorption, good fatigue resistance, and high temperature stability) compared to conventional aerospace materials. Polymer matrix composites have been used in some primary structural applications with great success, in both the military (B-2 Bomber, V-22 Osprey, etc.) and private industry (the Beech Starship, Airbus A320, etc.). Aerospace vehicles are beginning to contain more polymer matrix composites as load-bearing structures in order to lower weight. The DC-X has a nose section made of carbon/epoxy, the space shuttle external tank (ET) is scheduled to have a carbon/phenolic nosecap, and rocket motor cases have been made of fibrous composites for quite a while. Future use of polymer matrix composites has been identified for the hypersonic suborbital reusable booster (HSRB), X-2000, and National Aerospace Plane (NASP).

In order for a thermoset polymer to withstand high temperatures without a degradation of mechanical properties, a high cross-linking density is desired. However, a high cross-linking density will result in a brittle material that will not provide a damage-tolerant matrix for the composite. Some thermoplastic resins such as polyetheretherketone (PEEK), polybenzimidazole (PBI), and polyallylphenols can withstand higher temperatures than thermoset resins, and have the additional bonus of being inherently tough. However, thermoplastic matrix composites, which are difficult to handle since they have no tack or drape, require high temperatures and pressures to process. By blending thermoplastics into thermosets, the resulting polymer can be engineered to have a good balance of high temperature resistance, damage tolerance, and processability.

Epoxies are, by far, the most common matrix resin used for advanced composites. The first generation of epoxy resins was very brittle and did not possess good damage tolerance capabilities, thus limiting their use in critical load bearing applications. Newer-generation epoxy resins are "toughened" either by incorporating elastomeric particles or by alloying with tough thermoplastic polymers. The epoxies that are toughened via elastomeric particle dispersion offer greatly improved damage tolerance capabilities, but possess low hot/wet mechanical properties. Epoxies blended with thermoplastics show improved damage tolerance without losing as much hot/wet strength, thus making them more attractive for use in aerospace applications.

In applications where higher use temperatures are needed, polyimides are the most widely used thermoset resins. Polymerization of monomer reactants (PMR) is a polyimide developed at NASA's Lewis Research Center. The upper use temperature for this resin is about 600 °F, but processability is a problem since the prepreg has little tack and drape and needs cure pressures near 200 lb/in^2. This resin is commercially available as PMR-15. A newer resin, designated PMR-II, can be used at temperatures up to 660 °F, but it is also extremely difficult to process into useful shapes.[1] Another drawback with polyimides is their susceptibility to microcracking when thermally cycled. It has been shown that PMR-15 can lose compressive and interlaminar shear strength due to microcracking when cycled between 0 and 450 °F for 1,000 cycles.[2] Damage tolerance is another major

problem with PMR-15. In residual strength-after-impact testing of PMR-15 and 3501-6 resin/carbon fiber composites, the PMR-15 showed a higher reduction in residual flexural strength.[3]

A class of polyimides called bismaleimides (BMI's) have the processability of epoxies with the higher use temperatures common to polyimides. BMI's are polyimides that contain a vinyl group as part of the five-membered imide ring, resulting in an uncured prepreg that has good tack and drapeability and will process at 350 °F and 80 lb/in^2 (or lower), much like epoxies. Unlike epoxies, the BMI composite must undergo a free-standing postcure, usually at a temperature of about 475 °F for 8 h. BMI resins cannot match the temperature capabilities of PMR-15, since the upper use temperature of most BMI's is about 450 °F under dry conditions and 390 °F under wet conditions, but this is a substantial increase (about 200 °F) over epoxies. Like all polyimides, BMI is inherently brittle and must be modified with a "toughener" to be of any use as a matrix resin for advanced aerospace structures. Thus, about 25 to 50 percent by weight thermoplastic is blended with the BMI to improve its damage tolerance.[4] Some blends have demonstrated a resistance to microcracking when thermally cycled from −108 to 350 °F, making them as microcrack resistant as cyanate resin systems.[5] Different thermoplastics in a variety of amounts are used to engineer the matrix resin to have the most desirable properties for the application at hand. In general, BMI resins with the highest room temperature mechanical properties would be the most affected by heat, losing a larger percentage of strength with increasing temperature than those resins designed for hot environments which tend to have lower room temperature mechanical properties.[6] Most BMI resin systems are toughened with PBI since this thermoplastic has a glass transition temperature over 750 °F, although other thermoplastics such as polyetherimide (PEI) are used in some blends.[7 8]

This paper examines the impact resistance and damage tolerance of four aerospace grade polymer matrix systems that have been identified as candidate materials for the HSRB, NASP, and/or X-2000 programs. One of these systems is a toughened epoxy and the other three are toughened BMI resins. All of these materials contained the same fiber (Hercules' IM7) so a comparison of the matrix resins could be made without any type of reinforcement as an additional variable.

II. EXPERIMENTAL DESCRIPTION

A. Materials

1. *Material.* The four fiber/resin systems used in this impact damage tolerance study were IM7/977-2 epoxy, IM7/V390, IM7/V398, and IM7/F655 BMI's.

The 977-2 epoxy produced by ICI/Fiberite is the best characterized and most widely used toughened epoxy system. This epoxy resin contains about 10 percent by weight of a proprietary thermoplastic polymer.[9] Upon cure, a co-continuous morphology is obtained in which the thermoplastic and epoxy are distinct phases of interpenetrating polymer networks on the order of the submicron size.[10] The upper use temperature for this resin is about 250 °F, with use temperatures under wet conditions of 150 to 190 °F. Select mechanical properties for this composite are given in table 1.

The V390 and V398 BMI's are produced by Hitco and differ in their toughness and upper use temperature. The V390 resin possesses a hot/wet performance temperature of 475 °F while the tougher V398 resin has a hot/wet use temperature of 350 °F. Some mechanical properties for these

composites are given in tables 2 and 3 (note that the data for the V390 system were obtained with a different fiber than IM7).

The F655 BMI resin is produced by Hexcel and has an upper use temperature of 450 °F. This resin was designed primarily to have easy processing characteristics and enhanced damage tolerance. Table 4 shows some typical laminate composite properties for this resin system with IM6 fiber.

2. *Specimen Preparation.* Panels were made of unidirectional prepreg laid up in a quasi-isotropic stacking sequence of $[0,+45,90,-45]_{ns}$, where n was either 1, 2, or 3, thus producing 8-, 16-, or 24-ply laminates. The panels were hot-press cured according to the manufacturer's recommendations. Figure 1 shows the cure cycles used for the materials tested. Specimens 17.8-cm (7-in) long by 7.6-cm (3-in) wide were cut from the cured panels, and fiberglass end tabs 3.8-cm (1.5-in) long were bonded to the ends of each specimen as shown in figure 2. The cured nominal ply thicknesses for the various materials were 0.1219 mm (0.0048 in), 0.1372 mm (0.0054 in), 0.1168 mm (0.0046 in), and 0.1168 mm (0.0046 in) for the 977-2, F655, V390, and V398, respectively. These thicknesses correspond to the cure pressures used for the materials with the higher pressures giving thinner nominal ply thicknesses.

B. Testing

1. *Test Matrix.* A design-of-experiments approach was used to construct a test matrix that would evaluate the effects of impact level, plate thickness, and impactor diameter on the compression-after-impact (CAI) strength of the plates. Using such designed experiment techniques is becoming more prevalent due to the time and cost savings of reducing the number of destructive tests.[11] A Box-Behnken three-level fractional factorial design was implemented to minimize the number of tests needed to gather information about the effects of the three independent variables on the CAI strength. Utilizing this method, a total of 15 tests would need to be run on each material type. Each independent variable (impact level, plate thickness and impactor diameter) was assigned three values, representing a low, medium, and high setting. For the impact level, a low value was defined to be an incident kinetic energy of 4 J (2.95 ft-lb), a medium level was 8 J (5.90 ft-lb), and a high level was 12 J (8.85 ft-lb). The thickness of the specimen was determined by the three thicknesses fabricated, low = 8 plies, medium = 16 plies, and high = 24 plies. Tups of diameter 0.635, 1.27, and 1.9 cm (0.25, 0.5 and 0.75 in) were used as the low, medium, and high values of impactor size. The test matrix with the variables at the appropriate levels is shown in figure 3.

Utilizing the Box-Behnken technique would show all linear and quadratic effects of the three independent variables, as well as all two-way interactions between the variables that may exist.

2. *Impact Testing.* The specimens were pneumatically clamped between plates with cutout holes of 6.35-cm (2.5-in) diameter, thus inducing a circular clamped boundary condition. Each specimen was impacted at its geometric center. A Dynatup 8200 drop tower was used with a falling mass of 2.3 kg (5.0 lb). A catch mechanism was employed to prevent multiple strikes on the specimens. Instrumented impact data (such as incident impact velocity, maximum load of impact, total deflection, and energy absorbed during impact, as well as load-time and load-deflection plots for the impact event) were gathered with a Dynatup 730 data acquisition system. After each impact, the visual damage was noted and recorded.

3. *Nondestructive Evaluation (NDE).* After impact testing, all of the specimens were ultrasonically C-scanned to obtain a damage zone size. A double-through technique was used that

employs a DuPont transducer operating at a normal frequency of 5 MHz with a Testech receiver operating at an attenuation of 20 dB. The C-scans were then enlarged and marked into grids of size 2.54 mm (0.1 in) which corresponded to 2.27 mm (0.0896 in) of actual specimen area. The number of grids in the damage zone were counted to obtain a value for the total delamination area. The C-scans were color coded to represent the percentage of reflectivity of the ultrasonic pulses. When transformed into black/white format, the colors were represented by differing patterns on the resulting scan. For most of the specimens, the majority of the damaged area appeared as white (0-percent reflectivity) indicating delamination. For those specimens that had areas of nonzero reflectivity, any reflectivity below 50 percent was counted as part of the damage zone. These areas were restricted to the edges of the zone of delaminations and represented a small part of the overall damage area.

4. *Compression Testing.* Residual compressive strengths of the impacted specimens were obtained using a face-supporting, shear-loading technique explained in detail elsewhere.[12 13] Basically, this fixture is a large IITRI type with faceplates clamped lightly to most of the specimen's gauge length to prevent Euler buckling. The faceplates contained cutouts at their centers to allow the delaminations to "blister out" and grow. An Instron 1100 loading frame was used at a testing rate of 0.254 mm/min (0.01 in/min).

5. *Short-Beam Shear Testing.* Short-beam shear specimens were prepared from randomly selected, unimpacted 24-ply specimens. The specimens were 0.635-cm (0.25-in) wide, tested at a span of 1.27 cm (0.50 in). Testing was performed at a rate of 0.254 mm/min. (0.01 in/min).

6. *Double-Cantilever Beam Testing.* Double-cantilever beam (DCB) specimens were prepared from IM7/977-2 carbon/epoxy and IM7/V390 carbon/BMI material systems. Specimens were of a $[0,+45,90,-45]_{2S}$ lay-up, with a total length of 25.4 cm (10 in) and a width of 2.54 cm (1 in). A Teflon™ film insert was placed between the centermost 90/–45 interface at a distance of approximately 5 cm (2 in) from an end in order to obtain a starter crack. Testing was performed at a crosshead rate of 50 mm/min (2 in/min) and the value of G_{IC} was determined by the load/displacement area method.

C. General Results

1. *Impact Testing.* Results of the impact tests demonstrated that the variables chosen produced a range of visible damage from nondetectable to complete penetration for all of the material systems tested. Complete penetration occurred in all four material systems on runs No. 6 and 12, which corresponds to 8-ply specimens impacted at the highest level (12 J) with a 0.5 in diameter tup and a medium level impact (8 J) with the smallest diameter (0.25 in) tup. Run No. 3 produced no visible damage for all four material systems. This corresponds to the 16-ply laminate being impacted at the smallest level (4 J) with the largest (0.75 in) tup. All other impacts at this lower level were performed with smaller tups and produced damage that was detectable with the unaided eye.

The visible damage would first appear as a split along the back (nonimpacted) side of the plate, followed by a small dent at the impact site. As the impact conditions became more severe, the back-face splits would get wider and longer.

The thinner laminates showed more visible damage, and apparently the tup size does have an effect on the visible damage produced (a type of damage resistance), although less visual damage

may not translate into greater strength (damage tolerance) since compression strength is dominated by delaminations which are not detectable from the surface.

2. *NDE Testing.* All of the impacted specimens showed delaminations as indicated by the ultrasonic scanning results. All of the samples that were 16 or 24 plies thick showed circular areas of delamination. The 8-ply specimens showed delamination areas that were longer in the 0° (outer fiber) direction. This is due to the lower bending stiffness of the thinner laminates producing a much higher outer fiber membrane strain, which tended to break these fibers and split the matrix along the direction of these fibers. The area of delamination for each specimen is summarized in table 5, and the C-scans, along with maximum impact load and residual compression strength data, are presented in the appendix. A relatively large damage area is seen on the V390 and V398 specimens compared to the F655 and 977-2 resins for almost all of the runs. The only exceptions are the specimens that were completely penetrated by the impactor. In these cases, the apparently "tougher" 977-2 and F655 resins would resist splitting and cracking more, resulting in the broken fibers "carrying" more of the resin away from the laminate, resulting in delamination. The apparently less tough V390 and V398 resins would produce a "cleaner" hole when punctured since the resin would more easily crack and split, allowing the broken fibers to separate from the laminate with less far-field matrix damage. For the V398 and V390 samples that did not experience perforation, the damage zone extended to the boundaries of the circular clamp. This makes a true assessment of "damage resistance" difficult since the damage area would have been much greater had the delaminations not stopped at the clamped boundary. The 977-2 and F655 materials had delaminations that were contained well within the clamped boundary.

3. *Compression-After-Impact (CAI) Testing.* The results from the CAI tests are summarized in figures 4, 5, 6, and 7. All of the specimens failed at the impact site. The V390 and V398 resin system laminates do not have a noticeably lower CAI strength than the 977-2 and F655 resin system laminates, as would be expected from the NDE results. The drop in strength is not as large as would be indicated by the C-scans. The C-scans clearly show that the V390 and V398 resin laminates have a larger delamination area than the 977-2 and F655 resin laminates, but the V390 and V398 resin laminates do possess good damage tolerance since these large areas of damage do not cause a correspondingly large drop in compression strength. This phenomenon will be examined in detail later.

4. *Short-Beam Shear Testing.* A large difference in mode II interlaminar shear strength was evident between the materials tested. The delamination always initiated at one of the two center-most 90°/–45° interfaces. The results of the short-beam shear tests are given in figure 8. The V390 and V398 resin composites had much lower interlaminar shear strength than the F655 or 977-2 resin composites, which explains the larger delamination areas seen in the V390 and V398 resin laminates after impact.

As an indication of the consolidation between plies and the void content of the laminate, sections of some short-beam shear specimens were polished and photographed at 24× using a Zeiss stereomicroscope. These photographs are shown in figure 9. The only material that contains significant voids between plies is the IM7/F655. The other three materials all appear to have excellent consolidation. It should be noted that the F655 resin was processed at a lower pressure than the other resins (as called for by the manufacturer). However, this abnormality did not seem to adversely affect the mode II interlaminar shear strength as indicated by the short-beam shear tests. In fact, this material had a much higher interlaminar shear strength than the V390 and the V398 resin laminates.

5. *DCB Testing (G_{IC} Testing).* The V390 material was found to have a G_{IC} of approximately 0.92 kJ/m^2 (5.2 in-lb/in^2), and the 977-2 had a G_{IC} value of approximately 1.25 kJ/m^2 (7.3 in-lb/in^2). This difference is not as large as the difference in mode II shear strength as determined from the short-beam shear tests. Figure 10 shows photographs of the delamination growth of the IM7/977-2 and IM7/V390 DCB specimens. In all of the specimens, the delamination interface would grow from the 90/–45 interface, through the 90° ply to the 90/+45 interface. The delamination then grew to the +45/0 interface where stable crack growth occurred. The fact that planes of delamination growth will propagate to an interface that has fibers aligned in the direction of peeling has been found by other researchers.[14 15 16]

6. *Design of Experiments.* The CAI strength and area-of-damage results were considered the two dependent factors (responses) in the data analysis. The data analysis was performed using BNN Catalyst™ software set up to analyze a Box-Behnken design. The analysis resulted in a polynomial of the form:

$$\text{RESPONSE} = \text{CONTSTANT}+M_1(\text{Impact Energy})+M_2(\text{Thickness})+M_3(\text{Tup Size})$$

$$+M_{12}(\text{Impact Energy})(\text{Thickness})+M_{13}(\text{Impact Energy})(\text{Tup Size})$$

$$+M_{23}(\text{Thickness})(\text{Tup Size})+M_{11}(\text{Impact Energy})^2$$

$$+M_{22}(\text{Thickness})^2+M_{33}(\text{Tup Size})^2 \ ,$$

where the three independent variables where normalized from a high value of +1 to a low value of –1. A value of 0 indicates a medium setting of the variable. Thus, in the above expression, CONSTANT is the value of the response when all of the independent variables are at their medium settings. The M_i coefficients correspond to the linear effects of the three independent variables, the M_{ij} represent the coefficients of the two-way variable interaction terms, and the M_{ii} represent the coefficients of the quadratic contribution of each of the three independent variables. If any of the coefficients had a variability higher than the absolute value of the coefficient and if that coefficient was relatively small compared to the two highest coefficients, then that coefficient was removed, which resulted in better data with less "noise" for the other coefficients.

As an example, suppose the analysis gave the following coefficients for the CAI strength response: CONSTANT = 300, $M_1 = -30$, $M_2 = 20$, $M_3 = 5$, $M_{12} = -10$, $M_{13} = 0$, $M_{23} = 0$, $M_{11} = 40$, $M_{22} = 0$, $M_{33} = 0$. This would indicate that the M_{13}, M_{23}, M_{22}, and M_{33} terms were relatively small and/or had a high variability. The other terms were kept in the model and are interpreted as follows. The most influential term is M_{11} which has a value of 40. This is the coefficient for the quadratic influence of increasing impact energy, thus it can be assumed that the CAI strength of this material varies in a strong nonlinear form with the impact energy. The next most important term is the M_1 term with a value of –30. This is the coefficient for the linear dependence of CAI strength on increasing impact energy. Since this coefficient is negative, it indicates that as the impact energy increases, the CAI strength decreases. The only two-way interaction is found between impact energy and thickness. The coefficient for this term has a value of –10 and indicates that as the two variables go to their opposite extremes (one to its lowest value, the other to its highest), the value of the CONSTANT value will increase up to 10 units. As the two variables go to the same extremes (both go to their high or low values), then the CONSTANT value can decrease by 10 units.

To determine the output response at any combination within the values of the three independent variables selected, the independent values must be normalized to values between –1 and +1 like they are in figure 3. Suppose the tup was 0.25 inches in diameter, the specimen was 16-plies

thick and was impacted at 12 J of impact energy. The normalized values would be tup = −1, thickness = 0, and impact energy = +1. Putting these into the polynomial equation will result in:

$$\text{RESPONSE} = 300-30(+1)+20(0)+5(-1)-10(+1)(0)+0(+1)(-1)+0(0)(-1)$$

$$+40(+1)^2+0(0)^2+(0)(-1)^2 = 295 \ .$$

Now, suppose the impact energy was at 9 J, the tup size at 0.6 in, and the specimen at 8 plies. This would correspond to normalized values of impact energy = 0.25, tup = 0.4, and thickness = −1 which would give:

$$\text{RESPONSE} = 300-30(0.25)+(20)(-1)+5(0.4)-10(0.25)(-1)+0(0.25)(0.4)$$

$$+0(0.4)(-1)+40(0.25)^2+0(-1)^2+0(0.4)^2 = 279.5 \ .$$

Thus, the response can be predicted from the model for any combination of the three independent variables as long as these variable values are within the range tested.

III. EXPERIMENTAL RESULTS

A. Effects of Independent Variables

1. *IM7/977-2 Material.* The model terms for the CAI strength and damage area responses are given in table 6. There is a strong nonlinearity between the CAI response and the impact energy, as well as a strong negative linear effect. This can be seen on the response surface plot of CAI strength as a function of impact energy and specimen thickness, as shown in figure 11. There is a sharp drop in strength as the impact energy increases from the lowest level, but the strength decrease begins to level off near the higher end of impact energy with a slight increase in CAI strength seen at the highest impact energies. This is due to the specimen beginning to be punctured at these higher impact levels, resulting in more fiber damage and less matrix damage, which is the controlling factor for the residual compression strength of the laminate. There are not any significant two-way interactions for the CAI response, and the value of the tup setting is not significant for either of the responses. The damage zone is most heavily dependent on the linear impact energy coefficient, which indicates that as the impact energy increases, the area of damage also increases. This response also shows an interaction between impact energy and specimen thickness. As can be seen from figure 12, at the lower end of impact energies used in this study, the smallest damage areas occurred on the intermediate thickness specimens. The thick specimens had more flexural rigidity and, thus, could not absorb as much of the impact energy as bending strain energy, therefore causing this energy to be dissipated by matrix damage. The thinnest specimens could flex quite a bit, and the fibers would store plenty of elastic strain energy, but the deformations were large enough to cause matrix splitting between fibers, especially in the outer fiber direction, as is evident by the C-scans in the appendix. At the higher values of impact energy used in this study, the thinner the specimen the more damage area resulted. This is due to the fact that the tup would puncture the thinner specimens, resulting in gross fiber pullout along the outer fiber direction as is evident by the C-scans in the appendix. This larger area of damage contributed to a loss in CAI strength on the thin samples, as seen in figure 11, since the damage was completely through the thickness.

2. *IM7/F655 Material.* From figure 13, which is a response plot of CAI strength versus impact energy and specimen thickness, it can be seen that this material has a nonlinear dependence

on the impact energy. It has a similar shape to the IM7/977-2 composite CAI response in that the sharp drop in residual compression strength begins to level off at the higher end of impact energies used. The model terms are given in table 7. The linear coefficient of impact energy is the strongest term at –53 MPa, while the quadratic coefficient for this independent variable is 37 MPa. The linear thickness coefficient is quite large at 45 MPa with a quadratic coefficient of –15 MPa. This indicates that the thinner specimens had less strength than the thicker specimens, with this trend decreasing a small amount as the thickness increases (a leveling off). The tup size had a small effect on the CAI strength and damage area responses. A larger tup produced a larger CAI strength than the thinner tups, but this was dependent on the impact energy used, as is evident by the interaction term for both responses. In fact, the impact energy/tup size interaction term for the damage area response is greater than the linear or quadratic coefficients for the tup size on this response. Figure 14 shows the CAI strength response surface as a function of impact energy and tup size. At the high end of impact energy, the tup size had little effect on the CAI strength response and showed only a slight increase in strength with increasing tup size. However, at the lower impact energy levels, the tup size became more important and showed a larger increase in strength with increasing tup size. Figure 15 shows the damage area response surface as a function of impact energy and tup size. This plot indicates that at low values of impact energy, the smallest tup size gave the largest damage area, which corresponds with the CAI strength observations. However, at high impact energies, the damage area was much greater for the larger tup. This larger damage area did not correspond to a drop in CAI strength, mainly due to the results obtained on runs No. 1 and 2, which had the tup size at the two extremes and the largest impact energy used. Run No. 1 had a larger area of damage as detected by ultrasonics, but had a slightly higher CAI strength than the specimen in run No. 2. Since tup size does have an effect on the CAI strength, this material may have a compression failure mechanism that is not as heavily dependent on absolute two-dimensional (2–D) matrix damage size as epoxies, but is also dependent on the amount of through-the-thickness matrix damage and/or fiber breakage, since the smaller tup tended to break more fibers and cause more through-the-thickness matrix damage.

3. *IM7/V398 Material.* The model terms for this material (table 8) are quite different from the 977-2 and F655 resin systems, most notably the strong dependence of damage area on specimen thickness and the relatively smaller effect of impact energy on CAI strength. Figure 16 is a surface response plot of CAI strength as a function of impact energy and specimen thickness. This material is surprisingly insensitive to impact energy, especially on the thicker specimens. On the thinner specimens, a decrease in CAI strength is seen with an increase in impact energy. However, note that the quadratic impact energy coefficient is negative, which implies that a sharp drop in CAI strength is seen only at larger impact energies as the impact energy increases. This is the opposite trend from the 977-2 and F655 resin systems where, as the impact energy increased at larger values of impact energy, a puncture type of damage was formed and the drop in compressive strength began to level off. The trend in the V398 material suggests that the CAI strength may be more dependent on through-the-thickness damage and/or fiber breakage than absolute 2–D matrix damage size (a characteristic that was noticed to a small extent in the F655 material). The effects of specimen thickness on the CAI strength is very nonlinear, with the strength showing a rapid decrease as the specimen gets thinner, which again suggests that through-the-thickness damage and/or fiber breakage (which was more pronounced on the thinner specimens) has a strong influence on the CAI strength of the specimens.

The tup size also had an effect on the CAI strength of the specimens, as is evident by the plot in figure 17 which shows CAI strength as a function of impact energy and tup size. At the low levels of impact energy, the tup size had little effect on the residual compressive strength, but at the higher impact energies, a smaller tup would be more detrimental to the residual compression strength (a strong interaction coefficient shows this). Since the smaller tups tended to cause a puncture at the

higher impact energies than the larger tups, this again suggests that the CAI strength of this material is dependent upon the amount of through-the-thickness damage and/or fiber breakage and not on the absolute 2–D size of matrix damage as detected by C-scans.

The damage area caused by the impact was most influenced by the thickness of the specimen and little else, as is evident from the coefficients in table 8. The tup size had no effect on the damage area, and the impact energy had a small effect, but this response is clearly dominated by the specimen thickness, which can be graphically seen in figure 18. The damage area is linearly dependent on the specimen thickness with the thicker specimens showing much more damage area than the thinner specimens, regardless of impact energy (no interaction between these variables). As can be seen in the C-scans in the appendix, the thin specimens had a more elongated damage area, indicating matrix splitting, which is a through-the-thickness type of damage. The damage area varies nonlinearly with impact energy, with the lower impact energies giving less damage area. This trend leveled off around the medium values of impact energy, after which the impact energy had little effect on the measured damage area, since as mentioned earlier, the damage zone did not spread beyond the circular clamped boundaries of the plate.

4. *IM7/V390 Material.* The CAI strength of this material varies linearly with specimen thickness, the thicker specimens having a higher CAI strength. This dependence is quite significant, as is evidenced by the linear thickness coefficient seen in table 9 and the plot of CAI strength versus impact energy and specimen thickness shown in figure 19. The impact energy has a nonlinear effect on the CAI strength with the same trend seen as for the V398 material, and has a more pronounced effect on the residual compression strength at the higher impact energies. The "leveling off" of strength decrease is not at the higher end of impact energies as it is for most epoxies and the F655 BMI tested in this study. Another unique feature of this material is the effect of the tup size on the CAI strength of this material. The tup alone has no effects on the CAI strength, as can be seen by the zero coefficients for linear and quadratic tup terms in table 9. However, there are strong tup interaction terms with the other two variables. The interaction between tup size and impact energy can be seen in figure 20, which is a plot of CAI strength as a function of impact energy and tup size. At the small tup size, the impact energy shows a nonlinear drop in compression strength as the impact energy increases. When the tup is at the larger sizes, the CAI strength actually increases (albeit a very small amount) with increasing impact energy before a drop in strength is seen at the medium levels of impact. At the low levels of impact, increasing the tup size tended to decrease the CAI strength, a trend not seen in any of the other materials. But at the high impact levels, the larger tup showed little degradation of the CAI strength, especially when compared to the smaller tup sizes.

The tup size also had a strong interaction with the specimen thickness on the CAI response of the material, as can be seen in figure 21. At small tup sizes, the CAI strength did not depend heavily on the specimen thickness, but at large tup sizes, the CAI strength was much greater for thicker specimens. This once again indicated that specimens that have sustained fiber damage (those that have been punctured), such as thin specimens hit with a large tup or thicker specimens hit with a small tup, have a larger decrease in residual compression strength than those specimens that have sustained an impact where a heavy matrix damage area (not volume) has occurred, but little or no fiber breakage has occurred. The thin specimens saw a decrease in CAI strength as the tup was made larger, but the thicker specimens saw a decrease in CAI strength as the tup size became smaller. This can be explained by the thinner specimens sustaining a puncture type of damage regardless of tup size, thus a larger tup will produce a bigger hole resulting in more damage. For the thicker specimens, only the small tup could puncture the specimens and cause the fiber damage that seems to be associated with the decrease in the residual compressive strength.

The tup size had no effect on the damage size that was created due to the impact event except for a very small interaction with impact energy. The damage area was strongly dependent on the specimen thickness in a nonlinear manner, as is shown in figure 22, which is a plot of the response surface of damage size as a function of impact energy and specimen thickness. A sharp drop in damage area is seen as the specimen becomes thinner. This is due to a hole being punctured in the specimen and the damage being more localized in the form of fiber breakage and matrix splitting. For this reason the impact energy did not have as big an effect on damage size for the thin specimens as it did for the thicker specimens.

B. Comparison of Materials

1. *Damage Area.* A dramatic difference in damage area can be seen between the four materials tested. In general, the IM7/V398 and IM7/V390 materials sustained a much larger damage area than the IM7/977-2 and the IM7/F655 systems, especially for the thicker specimens. This is expected since the short-beam shear test results showed that the V398 and V390 materials had a much lower mode II delamination resistance.

2. *CAI Strength.* The CAI strength of the materials tested did not vary nearly as much as the damage area. The low mode II shear strength and large delamination areas of the V398 and V390 systems did not translate into large reductions in CAI strength. In fact, the V398 and V390 systems had the highest CAI strengths when all three independent variables were set at their medium settings (the "CONSTANT" values given in tables 6, 7, 8, and 9). The V398 and V390 systems, while not appearing to be very damage resistant, were very damage tolerant since they retained compression-after-impact strength well, even when the ultrasonic scans showed large areas of matrix damage. There is strong evidence that the BMI systems, especially the V398 and V390, have a compression failure mechanism that is related to the amount of through-the-thickness damage (damage volume) and not the amount of matrix damage area as detected by the ultrasonic scans.

3. *CAI Strength Versus Damage Area.* Figures 23, 24, and 25 show plots of CAI strength versus delamination area for the 8-, 16-, and 24-ply specimens. For the 8-ply specimens, there is little correlation between damage area and CAI strength. For the 16- and 24-ply specimens, the 977-2 and F655 systems show a much lower CAI strength as the damage area increases. For the V390 and V398 resins, however, the CAI strength is relatively independent of damage size.

IV. ANALYSIS OF RESULTS

A. Summary of Experimental Results

From the experimental data, the following can be concluded;

- The V398 and V390 laminates behave similarly and the F655 and 977-2 laminates behave similarly in both the CAI and damage area developed. The two sets behave quite differently.

- The V398 and V390 resin systems have a much lower mode II delamination resistance and, thus, produce larger damage zones as detected by ultrasonic scanning. This does not apply to the 8-ply specimens since they experience a puncture type of damage (fiber breakage and/or longitudinal matrix splitting).

- The V398 and V390 materials do not have as large of a drop in CAI strength as the 977-2 and F655 materials.

- The 977-2 and F655 laminates have "classical" CAI versus impact level plots (i.e., the strength drops off sharply at the early stages of damage and then levels off with increasing impact energy). The V398 and V390 laminates show no sharp drop in CAI strength until high levels of impact are reached.

- The V398 (and to a lesser extent the V390) 16- and 24-ply laminates show very little change in CAI strength regardless of damage size.

- Cross-sectional examination of the impact zone shows that the V390 and V398 laminates have large delaminations with little matrix cracking. The 977-2 and F655 laminates had damage within more plies (more through-the-depth damage), but the delamination sizes were very small compared to the V390 and V398 laminates.

V. RECOMMENDATIONS

From a damage tolerance standpoint, the V390 and V398 resin composites would be better suited for structural applications for the following reasons:

- The V398 and V390 resin composites had a much smaller drop in CAI strength with increasing impact levels, which would make in-service impacts less of a concern.

- The V398 and V390 resin composites showed a much larger area of damage via ultrasonic scanning (with little decrease in compression strength) than the F655 or 977-2 resin composites. This would mean easier detection in the field as a part is undergoing NDE inspection.

- The V398 and V390 resins are BMI's and can withstand higher service temperatures than epoxies such as the 977-2.

- The extensive "through-the-thickness" damage seen in the F655 and 977-2 resin composites is much more difficult to detect by NDE methods and appears to contribute to a significant loss in CAI strength.

Table 1. Select mechanical properties for IM7/977-2 (from reference 13).

Mechanical Property	70 °F	190 °F	220 °F	250 °F	180 °F Wet	190 °F Wet	220 °F Wet
0° Tensile Strength (ksi)	409						
0° Tensile Modulus (Msi)	25.1						
90° Tensile Strength (ksi)	10.9						
90° Tensile Modulus (Msi)	1.1						
0° Compression Strength (ksi)	234	225	217	214	192	185	175
0° Compression Modulus (Msi)	22.8	23.0	21.4	22.7	22.2	21.6	22.6
Short-Beam Shear Strength (ksi)	16.3	13.5	12.7	11.4	12.3	11.8	10.0
In-Plane Shear Strength (ksi)	15.8	15.3	14.6	14.1	14.5	14.1	13.9
In-Plane Shear Modulus (Msi)	0.80	0.72	0.68	0.69	0.67	0.64	0.59

Table 2. Select mechanical properties for IM7/V398 (from vendor).

Mechanical Property	70 °F	350 °F	350 °F Wet
0° Tensile Strength (ksi)	422		
0° Tensile Modulus (Msi)	23.3		
0° Compression Strength (ksi)	249	234	172
0° Compression Modulus (Msi)	22.7	22.1	22.0
Short-Beam Shear Strength (ksi)	20.5	15.0	8.7

Table 3. Select mechanical properties for Hitex 46-8B/V390 (from vendor).

Mechanical Property	70 °F	450 °F	450 °F Wet	600 °F
0° Tensile Strength (ksi)	371	368		
0° Tensile Modulus (Msi)	26.2	26.8		
0° Compression Strength (ksi)	286	177	172	
0° Compression Modulus (Msi)	24.6	24.4	22.0	
Short-Beam Shear Strength (ksi)	16.8	10.1	7.4	6.3

Table 4. Select mechanical properties for IM6/F655 (from vendor).

Mechanical Property	70 °F	350 °F	450 °F	350 °F Wet	450 °F Wet
0° Tensile Strength (ksi)	398	368			
0° Tensile Modulus (Msi)	24	26.8			
0° Flexure Strength (ksi)	270	189	158	133	
0° Flexure Modulus (Msi)	21.0	19.8	20.2	19.0	
Short-Beam Shear Strength (ksi)	17.1	12.9	9.4	6.5	3.9

Table 5. Damage area from C-scans of specimens impact tested.

Specimen No.	Delamination area in cm^2 (in^2)			
	IM7/V390	IM7/V398	IM7/F655	IM7/977-2
1	45 (7.0)	36 (5.6)	23 (3.6)	9 (1.4)
2	45 (6.9)	39 (6.0)	10 (1.5)	11 (1.7)
3	30 (4.7)	23 (3.5)	3 (0.5)	3 (0.5)
4	21 (3.2)	12 (1.8)	3 (0.5)	3 (0.5)
5	44 (6.8)	40 (6.2)	11 (1.7)	11 (1.7)
6	14 (2.1)	9 (1.4)	14 (2.1)	19 (2.9)
7	20 (3.1)	45 (6.9)	3 (0.4)	2 (0.3)
8	5 (0.8)	5 (0.8)	5 (0.8)	3 (0.5)
9	41 (6.3)	73 (11.3)	7 (1.1)	7 (1.1)
10	9 (1.4)	8 (1.3)	11 (1.7)	8 (1.2)
11	40 (6.2)	56 (8.7)	6 (0.9)	7 (1.1)
12	9 (1.4)	8 (1.2)	8 (1.3)	8 (1.3)
13	43 (6.6)	43 (6.6)	7 (1.1)	7 (1.1)
14	44 (6.8)	48 (7.5)	8 (1.2)	7 (1.1)
15	41 (6.3)	41 (6.3)	7 (1.1)	8 (1.2)

Table 6. Model terms for IM7/977-2 material.

RESPONSE		Linear coefficients			Interaction Coefficients			Quadratic Coefficients		
					Impact Energy	Impact Energy	Thickness	Impact Energy	Thickness	Tup Size
	CONSTANT	Impact Energy	Thickness	Tup Size	Thickness	Tup Size	Tup Size	Impact Energy	Thickness	Tup Size
CAI (Mpa)	293	–44	34.5	0	0	0	0	50	0	0
Damage Area (cm^2)	6.6	4.9	–1.4	0	–1.8	0	0	0	1.5	0

Table 7. Model terms for IM7/F655 material.

RESPONSE		Linear coefficients			Interaction Coefficients			Quadratic Coefficients		
					Impact Energy	Impact Energy	Thickness	Impact Energy	Thickness	Tup Size
	CONSTANT	Impact Energy	Thickness	Tup Size	Thickness	Tup Size	Tup Size	Impact Energy	Thickness	Tup Size
CAI (Mpa)	318	–53	45	11	11	–7	0	37	–15	0
Damage Area (cm^2)	6.7	5.5	–1.4	2.1	0	3.2	0	1.6	0	1.4

Table 8. Model terms for IM7/V398 material.

RESPONSE		Linear coefficients			Interaction Coefficients			Quadratic Coefficients		
					Impact Energy	Impact Energy	Thickness	Impact Energy	Thickness	Tup Size
	CONSTANT	Impact Energy	Thickness	Tup Size	Thickness	Tup Size	Tup Size	Impact Energy	Thickness	Tup Size
CAI (Mpa)	352	-14.5	40	9.6	14.5	21	0	-11	-38	0
Damage Area (cm^2)	38	4.9	23	0	0	0	0	-12	0	0

Table 9. Model terms for IM7/V390 material.

RESPONSE		Linear coefficients			Interaction Coefficients			Quadratic Coefficients		
					Impact Energy	Impact Energy	Thickness	Impact Energy	Thickness	Tup Size
	CONSTANT	Impact Energy	Thickness	Tup Size	Thickness	Tup Size	Tup Size	Impact Energy	Thickness	Tup Size
CAI (Mpa)	323	-16	25	0	0	20.5	21	-29	0	0
Damage Area (cm^2)	40.9	9.0	13.5	0	3.8	-2.2	0	-5.1	-15.6	0

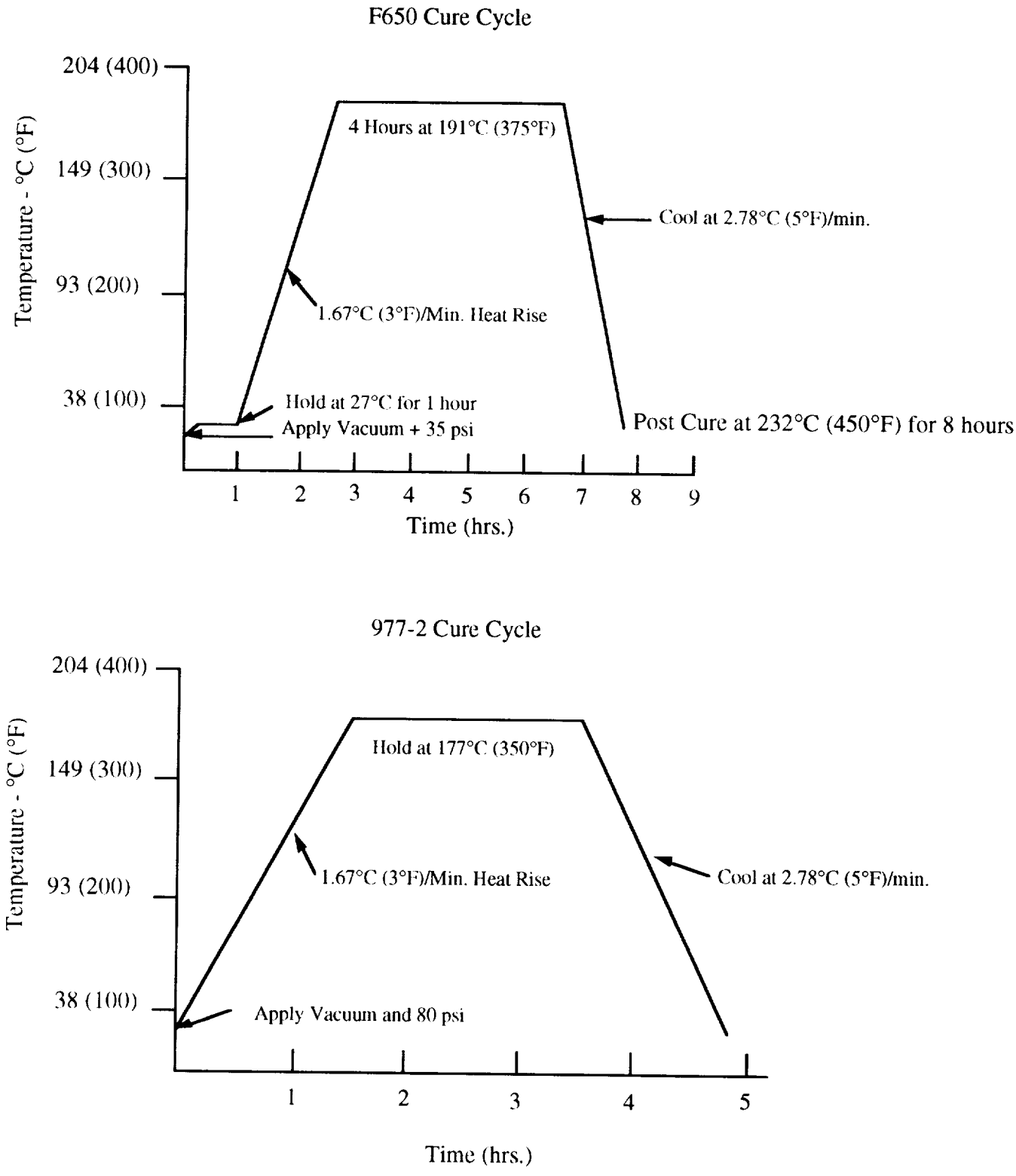

Figure 1. Cure cycles for F655 BMI and 977-2 epoxy.

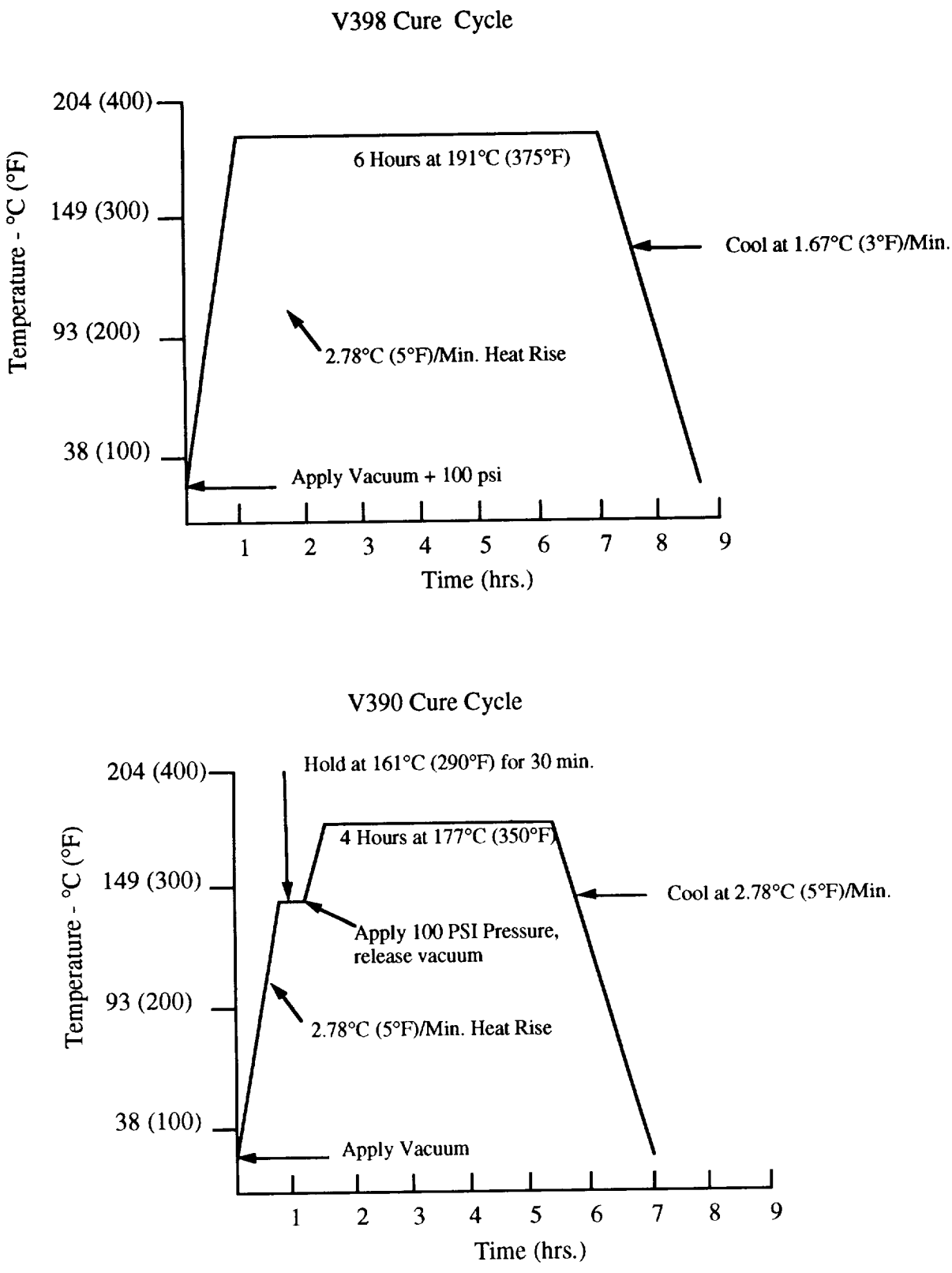

Figure 1. Cure cycles for V398 BMI and V390 BMI (continued).

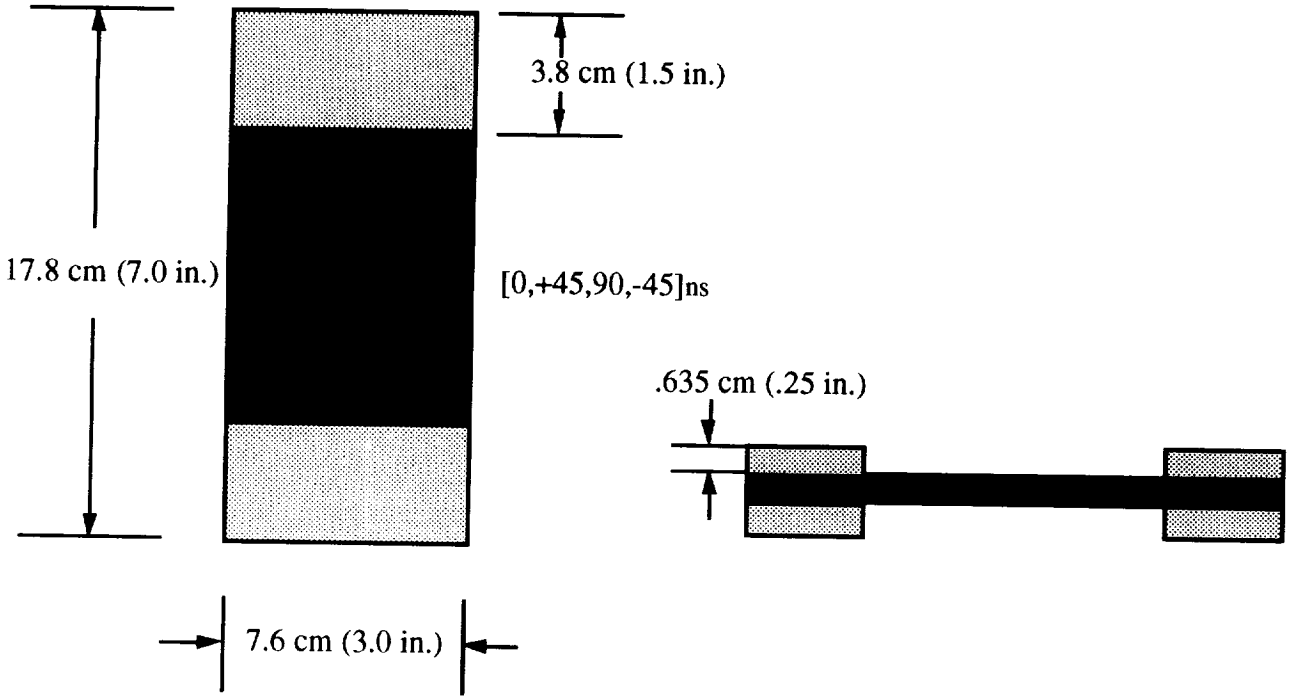

Figure 2. Compression-after-impact (CAI) specimens used in this study.

Run No.	Impact Energy	Thickness	Tup Size
1	+1	0	+1
2	+1	0	−1
3	−1	0	+1
4	−1	0	−1
5	+1	+1	0
6	+1	−1	0
7	−1	+1	0
8	−1	−1	0
9	0	+1	+1
10	0	−1	+1
11	0	+1	−1
12	0	−1	−1
13	0	0	0
14	0	0	0
15	0	0	0

−1 = 4 J	−1 = 8 plies	−1 = 0.25 in
0 = 8 J	0 = 16 plies	0 = 0.5 in
+1 = 12 J	+1 = 24 plies	+1 = 0.75 in

Figure 3. Run summary for impact tests.

Specimen No.	No. of plies	Tup Size cm (in)	Impact Energy J (ft-lbs)	CAI Strength MPa (lb/in^2)
1	16	1.9 (0.75)	12 (8.85)	304 (44,059)
2	16	0.64 (0.25)	12 (8.85)	287 (41,584)
3	16	1.9 (0.75)	4 (2.95)	410 (59,488)
4	16	0.64 (0.25)	4 (2.95)	380 (55,116)
5	24	1.27 (0.50)	12 (8.85)	327 (47,483)
6	8	1.27 (0.50)	12 (8.85)	276 (40,087)
7	24	1.27 (0.50)	4 (2.95)	407 (59,000)
8	8	1.27 (0.50)	4 (2.95)	349 (50,712)
9	24	1.9 (0.75)	8 (5.90)	313 (45,470)
10	8	1.9 (0.75)	8 (5.90)	212 (30,749)
11	24	0.64 (0.25)	8 (5.90)	344 (49,889)
12	8	0.64 (0.25)	8 (5.90)	278 (40,381)
13	16	1.27 (0.50)	8 (5.90)	319 (46,358)
14	16	1.27 (0.50)	8 (5.90)	306 (44,463)
15	16	1.27 (0.50)	8 (5.90)	325 (47,103)

Figure 4. CAI test results for IM7/977-2 material systems.

Specimen No.	No. of plies	Tup Size cm (in)	Impact Energy J (ft-lbs)	CAI Strength MPa (lb/in^2)
1	16	1.9 (0.75)	12 (8.85)	310 (45,036)
2	16	0.64 (0.25)	12 (8.85)	294 (42,632)
3	16	1.9 (0.75)	4 (2.95)	432 (62,639)
4	16	0.64 (0.25)	4 (2.95)	389 (56,467)
5	24	1.27 (0.50)	12 (8.85)	338 (49,012)
6	8	1.27 (0.50)	12 (8.85)	236 (34,214)
7	24	1.27 (0.50)	4 (2.95)	420 (61,000)
8	8	1.27 (0.50)	4 (2.95)	362 (52,483)
9	24	1.9 (0.75)	8 (5.90)	365 (53,015)
10	8	1.9 (0.75)	8 (5.90)	258 (37,525)
11	24	0.64 (0.25)	8 (5.90)	344 (49,948)
12	8	0.64 (0.25)	8 (5.90)	249 (36,087)
13	16	1.27 (0.50)	8 (5.90)	306 (44,367)
14	16	1.27 (0.50)	8 (5.90)	323 (46,940)
15	16	1.27 (0.50)	8 (5.90)	311 (45,181)

Figure 5. CAI test results for IM7/F655 material system.

Specimen No.	No. of plies	Tup Size cm (in)	Impact Energy J (ft-lbs)	CAI Strength MPa (lb/in^2)
1	16	1.9 (0.75)	12 (8.85)	310 (45,045)
2	16	0.64 (0.25)	12 (8.85)	245 (35,556)
3	16	1.9 (0.75)	4 (2.95)	303 (44,000)
4	16	0.64 (0.25)	4 (2.95)	320 (46,578)
5	24	1.27 (0.50)	12 (8.85)	326 (47,273)
6	8	1.27 (0.50)	12 (8.85)	231 (33,504)
7	24	1.27 (0.50)	4 (2.95)	341 (49,515)
8	8	1.27 (0.50)	4 (2.95)	278 (40,351)
9	24	1.9 (0.75)	8 (5.90)	357 (51,800)
10	8	1.9 (0.75)	8 (5.90)	295 (42,850)
11	24	0.64 (0.25)	8 (5.90)	313 (45,455)
12	8	0.64 (0.25)	8 (5.90)	334 (48,495)
13	16	1.27 (0.50)	8 (5.90)	301 (43,733)
14	16	1.27 (0.50)	8 (5.90)	326 (47,289)
15	16	1.27 (0.50)	8 (5.90)	325 (47,200)

Figure 6. CAI test results for IM7/V390 material system.

Specimen No.	No. of plies	Tup Size cm (in)	Impact Energy J (ft-lbs)	CAI Strength MPa (lb/in^2)
1	16	1.9 (0.75)	12 (8.85)	357 (51,877)
2	16	0.64 (0.25)	12 (8.85)	295 (42,845)
3	16	1.9 (0.75)	4 (2.95)	349 (50,608)
4	16	0.64 (0.25)	4 (2.95)	371 (53,873)
5	24	1.27 (0.50)	12 (8.85)	351 (50,933)
6	8	1.27 (0.50)	12 (8.85)	229 (33,273)
7	24	1.27 (0.50)	4 (2.95)	346 (50,228)
8	8	1.27 (0.50)	4 (2.95)	282 (40,991)
9	24	1.9 (0.75)	8 (5.90)	354 (51,383)
10	8	1.9 (0.75)	8 (5.90)	296 (43,000)
11	24	0.64 (0.25)	8 (5.90)	344 (49,985)
12	8	0.64 (0.25)	8 (5.90)	269 (39,064)
13	16	1.27 (0.50)	8 (5.90)	350 (50,789)
14	16	1.27 (0.50)	8 (5.90)	364 (52,780)
15	16	1.27 (0.50)	8 (5.90)	323 (46,913)

Figure 7. CAI test results for IM7/V398 material system.

Material	Interlaminar Shear Stress lb/in^2 (90°/–45°) Interface
IM7/977-2	13,167
IM7/F655	12,404
IM7/V390	6,123
IM7/V398	8,820

Figure 8. Short-beam shear results.

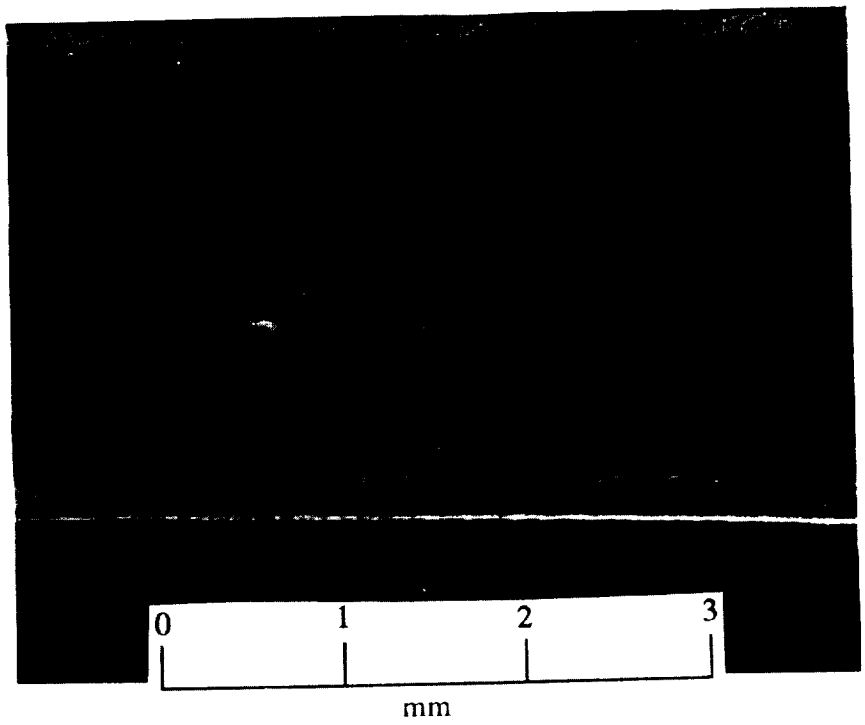

IM7/977-2 24 ply

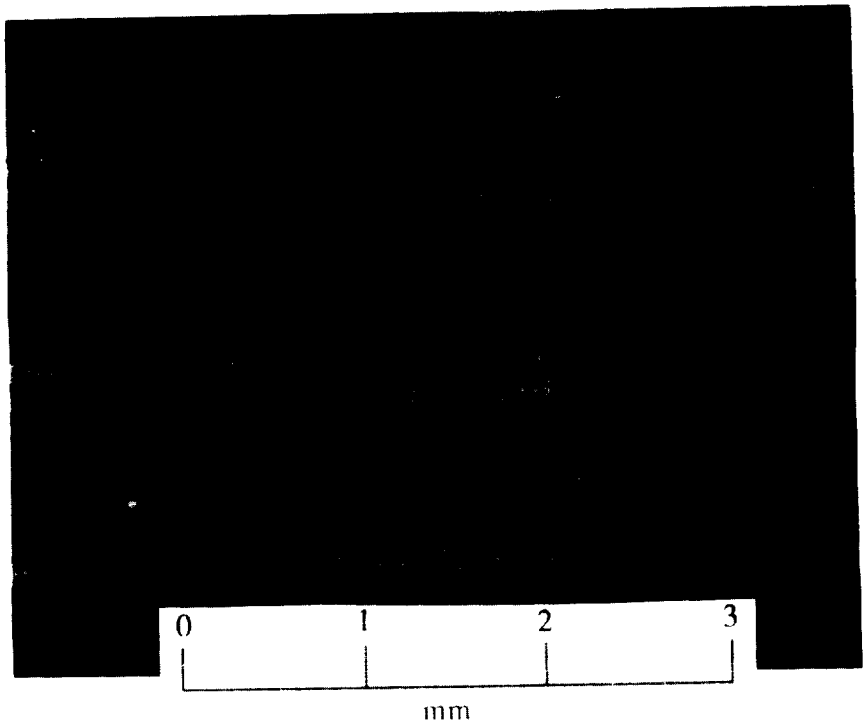

IM7/F655 24 ply

Figure 9. Cross-sections of the four material systems used (24× magnification).

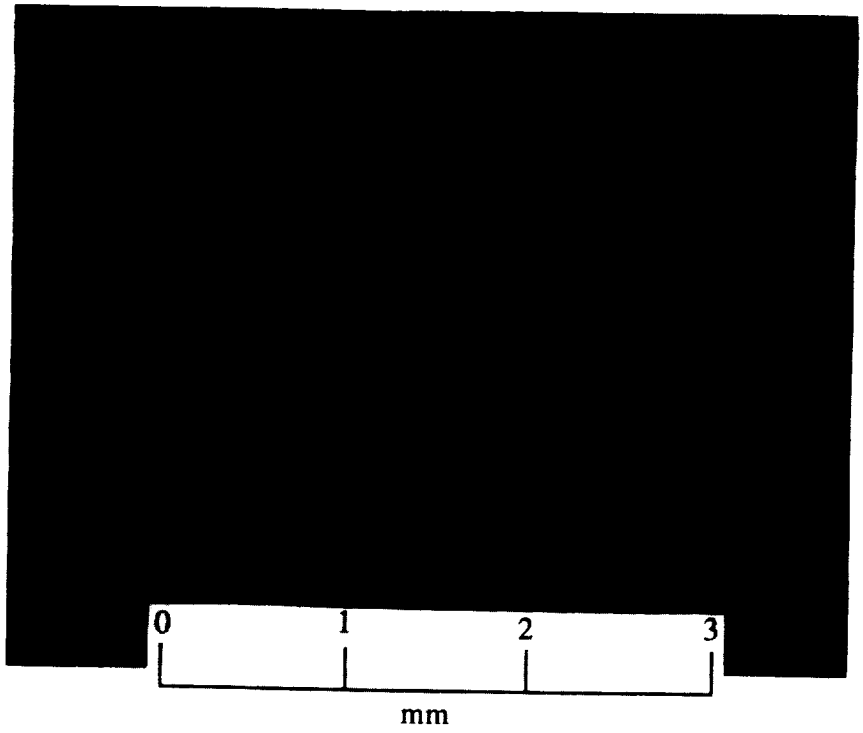

IM7/V398 24 ply

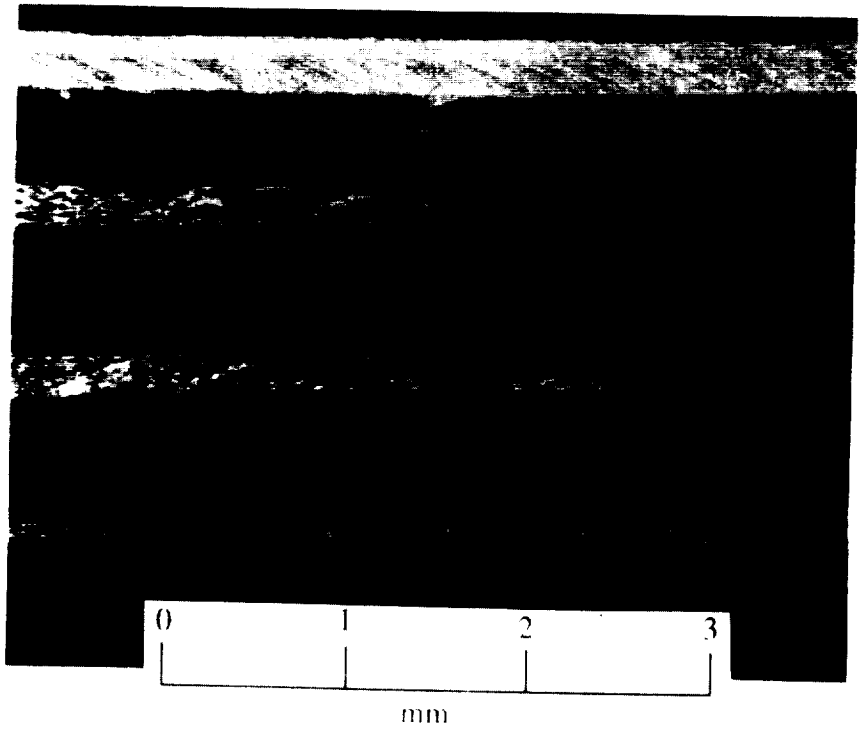

IM7/V390 24 ply

Figure 9. Cross-sections of the four material systems used (24× magnification) (continued).

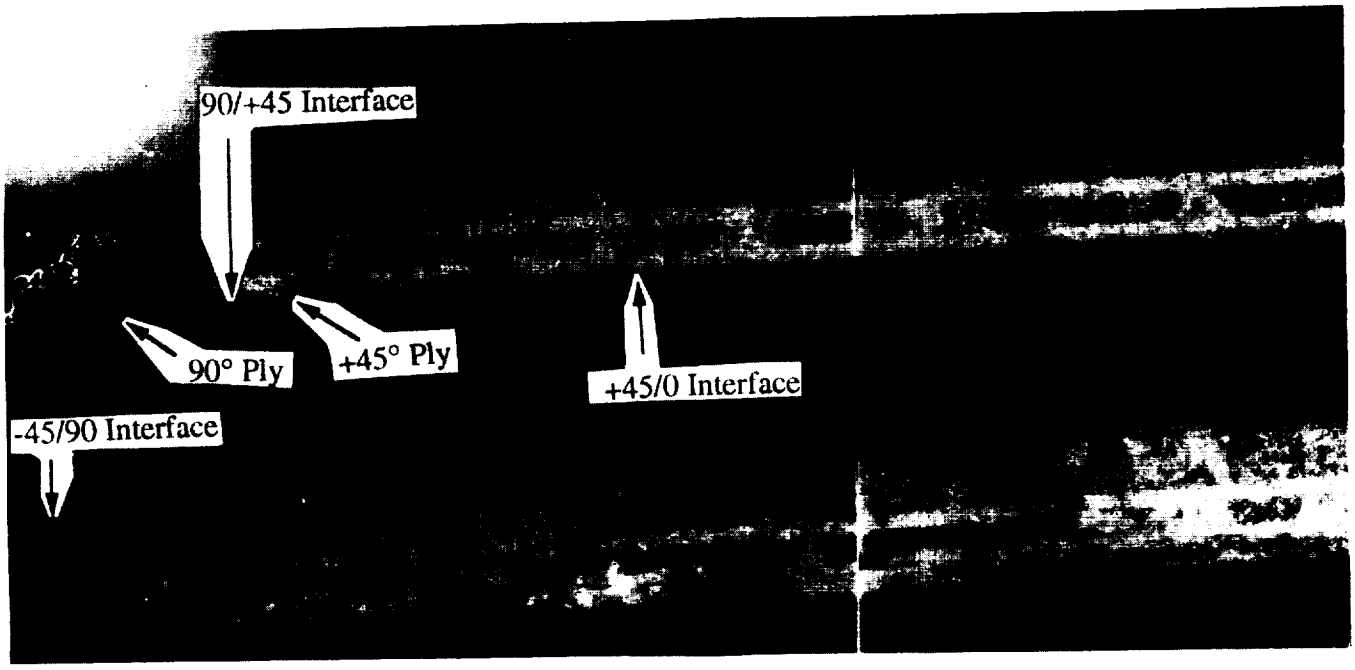

IM7/977-2

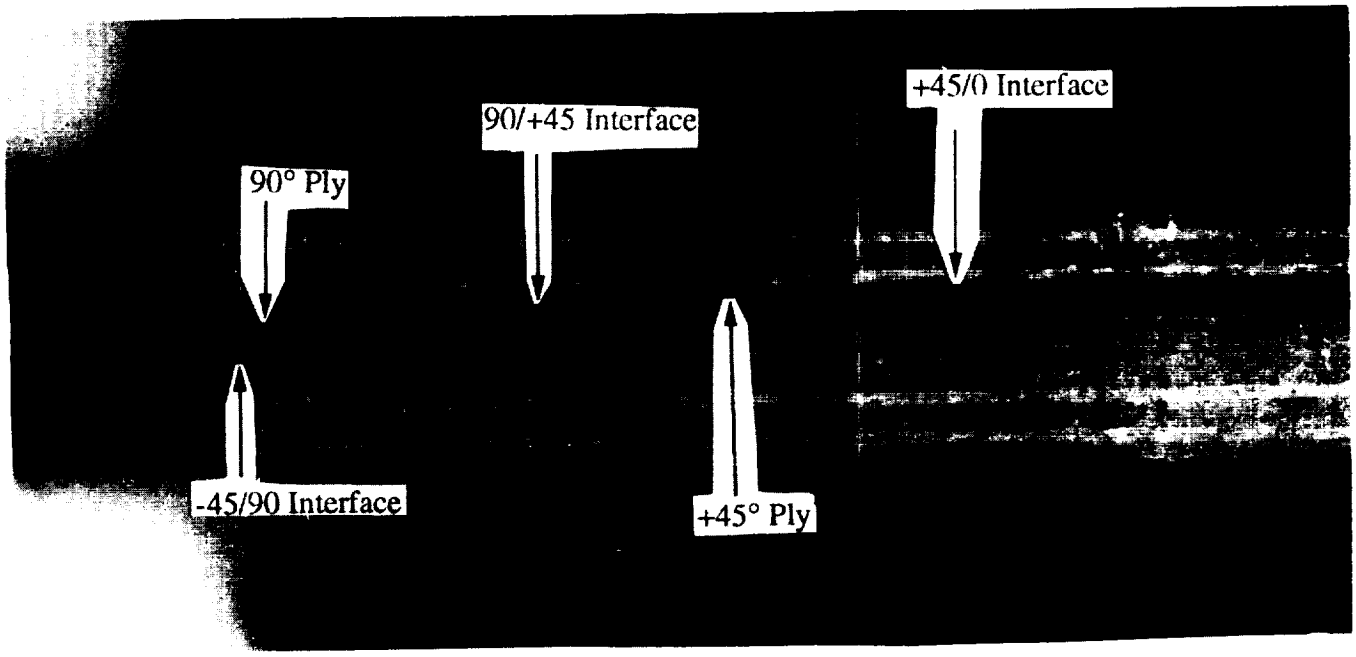

IM7/V390

Figure 10. Double cantilever beam test specimens; IM7/977-2 and IM7/V390.

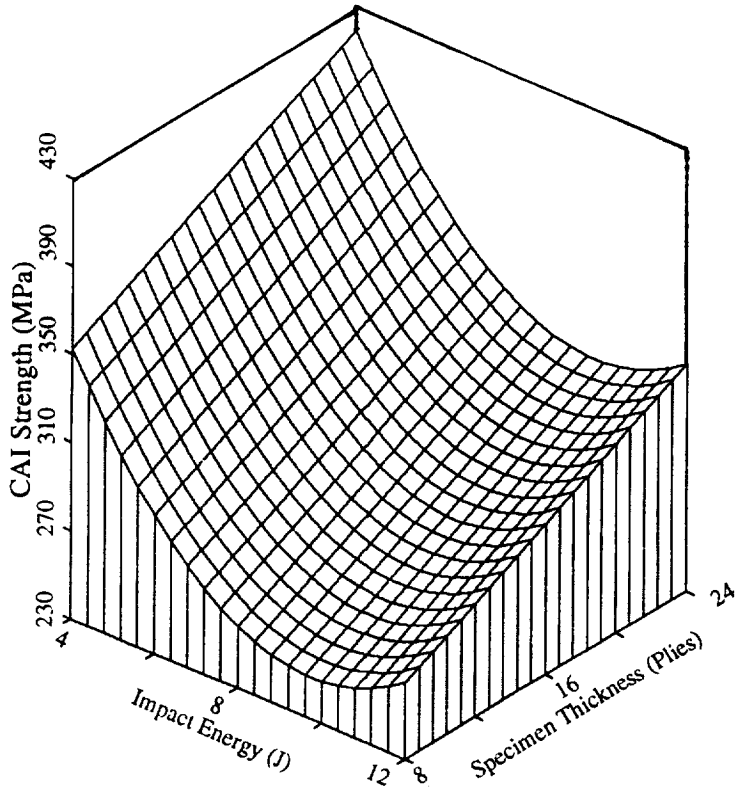

Figure 11. Compression-after-impact strength versus specimen thickness and impact energy for IM7/977-2.

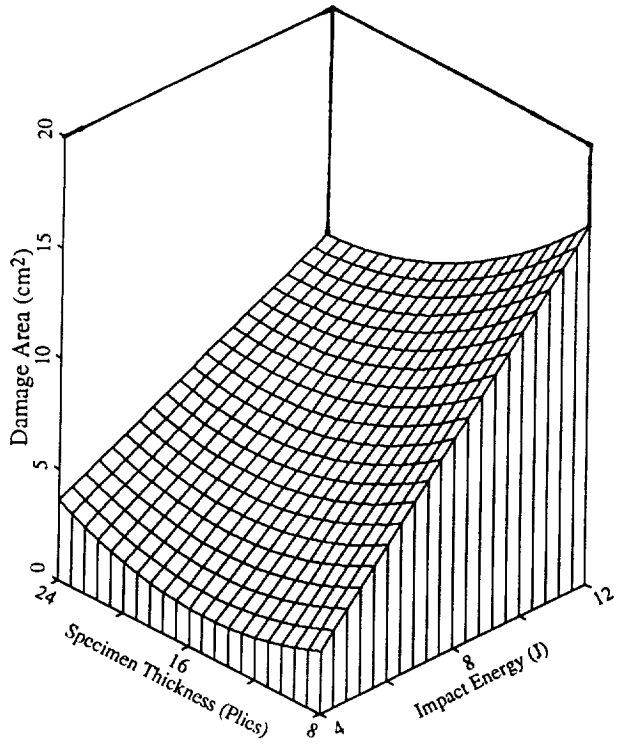

Figure 12. Damage area versus specimen thickness and impact energy for IM7/9770-2.

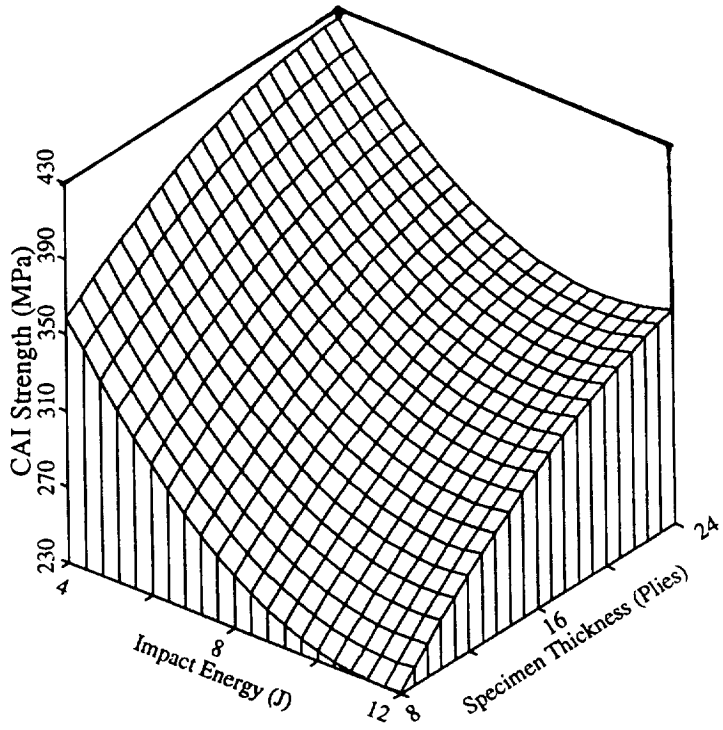

Figure 13. Compression-after-impact strength versus specimen thickness and impact energy for IM7/F655.

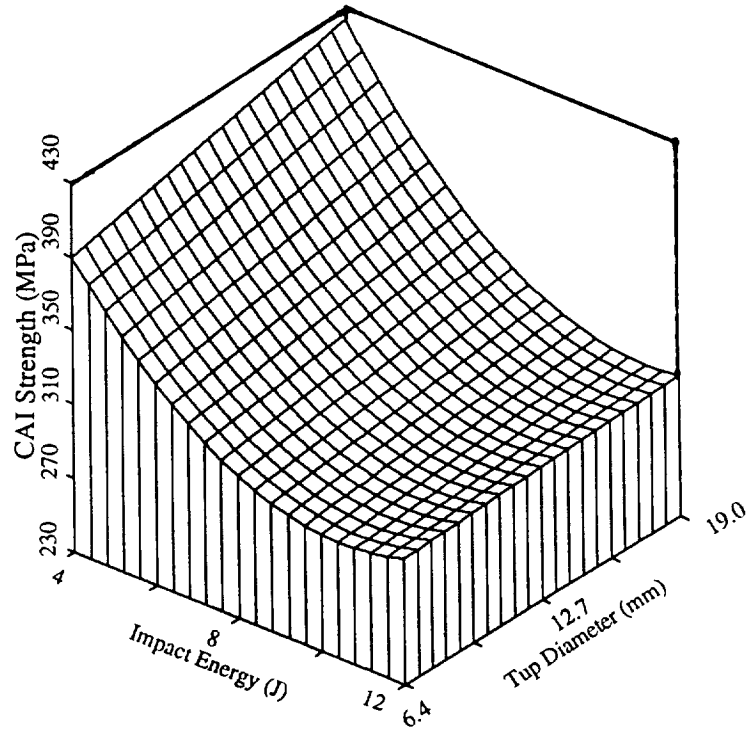

Figure 14. Compression-after-impact strength versus tup size and impact energy for IM7/F655.

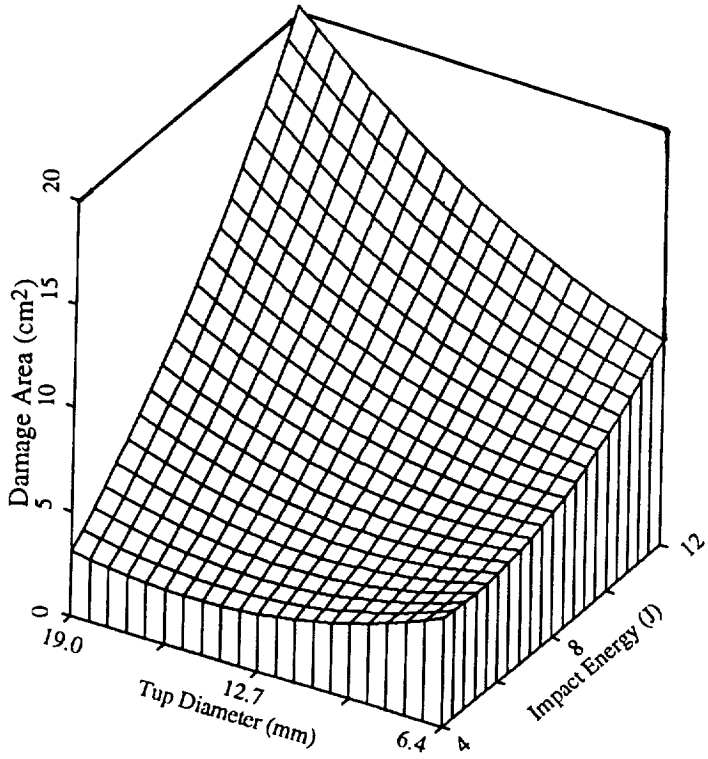

Figure 15. Damage area versus tup size and impact energy for IM7/655.

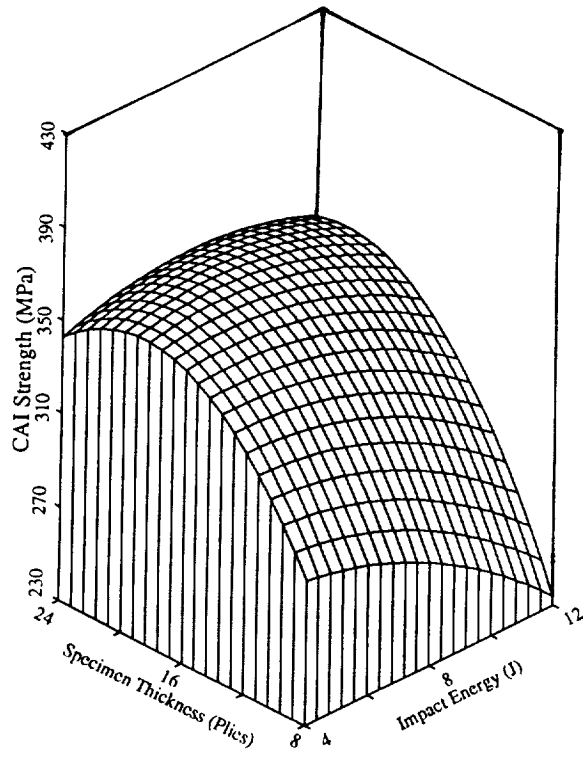

Figure 16. Compression-after-impact strength versus specimen thickness and impact energy for IM7/V398.

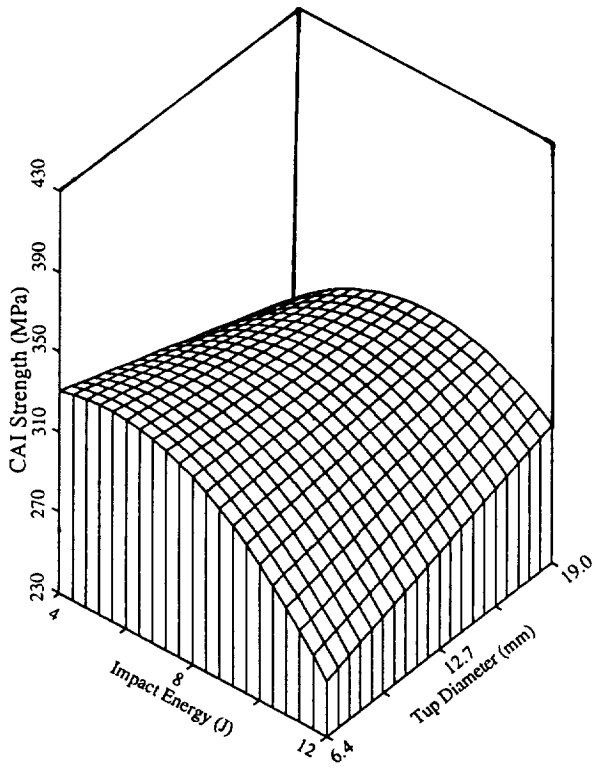

Figure 17. Compression-after-impact strength versus tup size and impact energy for IM7/V398.

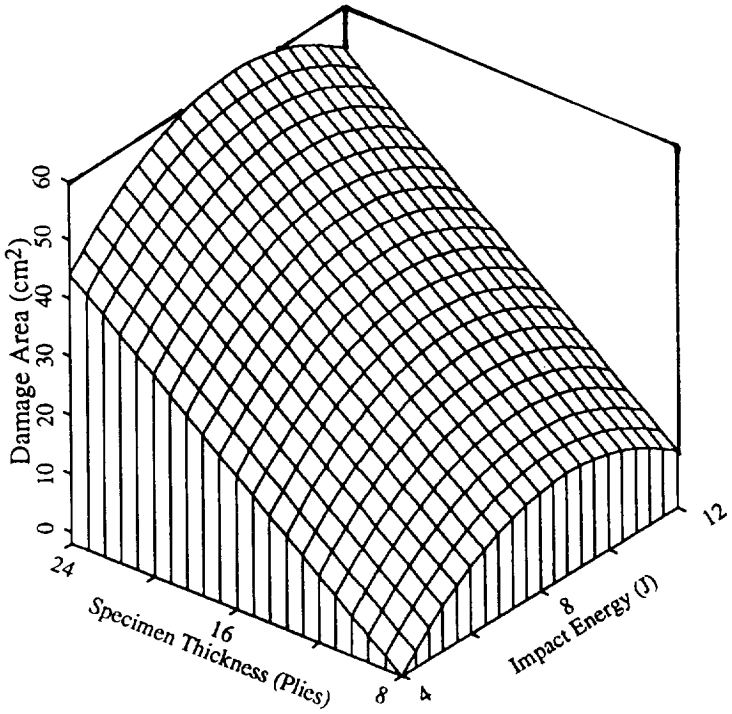

Figure 18. Damage area versus specimen thickness and impact energy for IM7/V398.

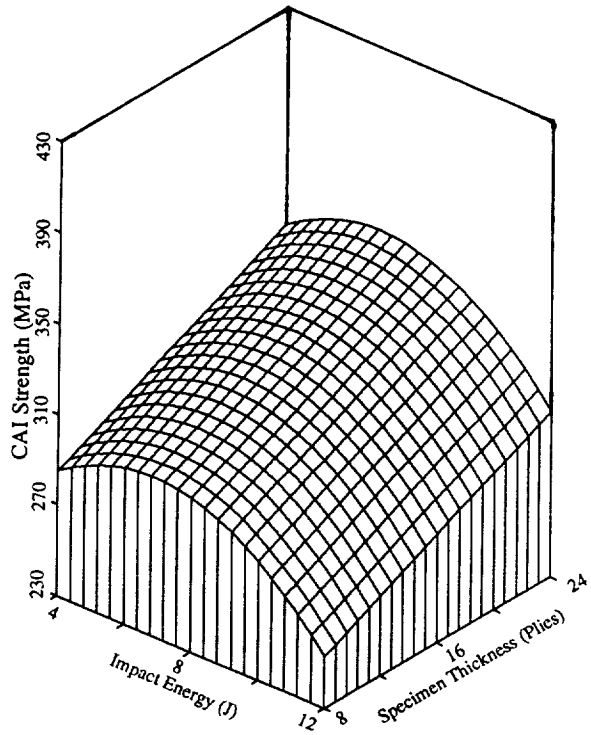

Figure 19. Compression-after-impact strength versus specimen thickness and impact energy for IM7/V390.

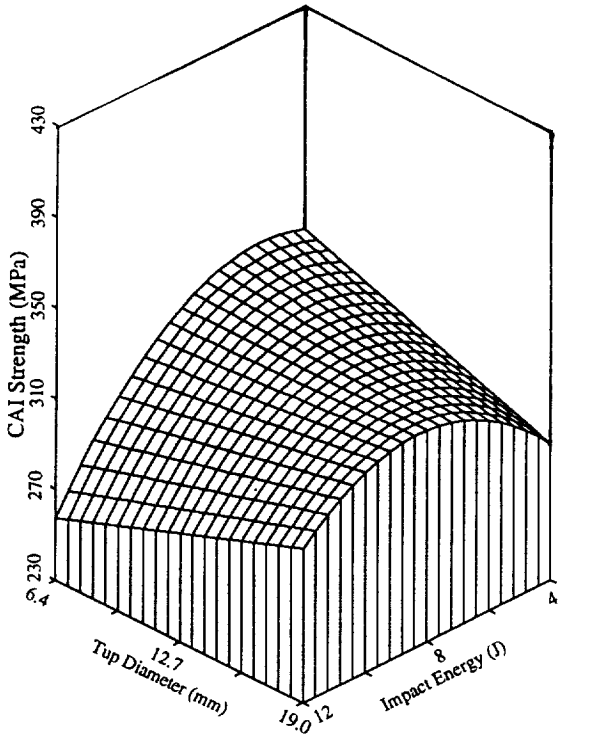

Figure 20. Compression-after-impact strength versus tup size and impact energy for IM7/390.

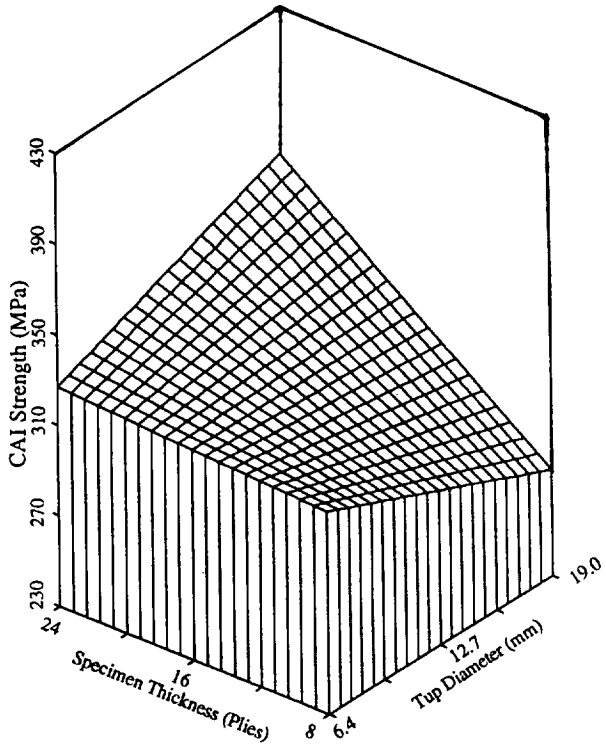

Figure 21. Compression-after-impact strength versus tup size and specimen thickness for IM7/V390.

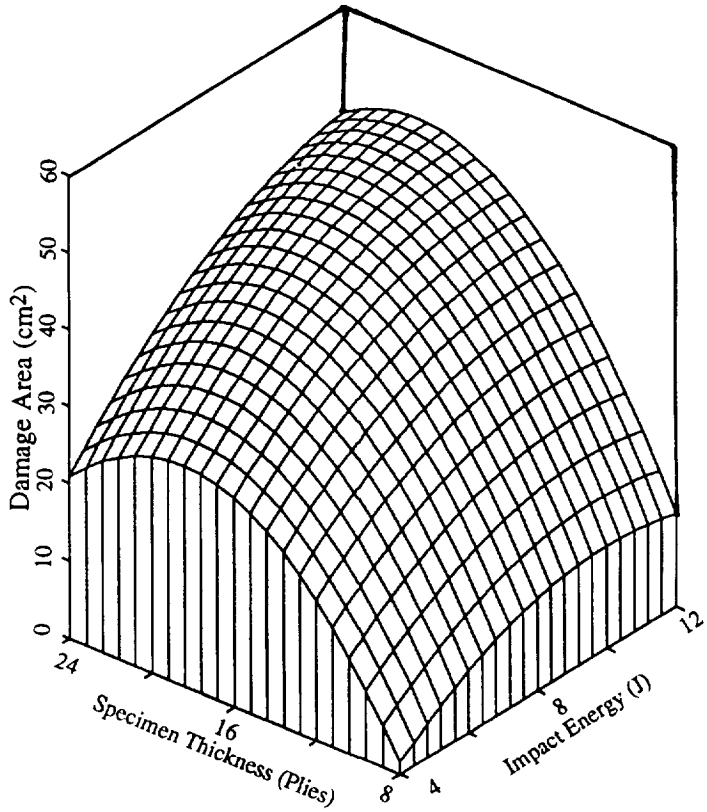

Figure 22. Damage area versus specimen thickness and impact energy for IM7/V390.

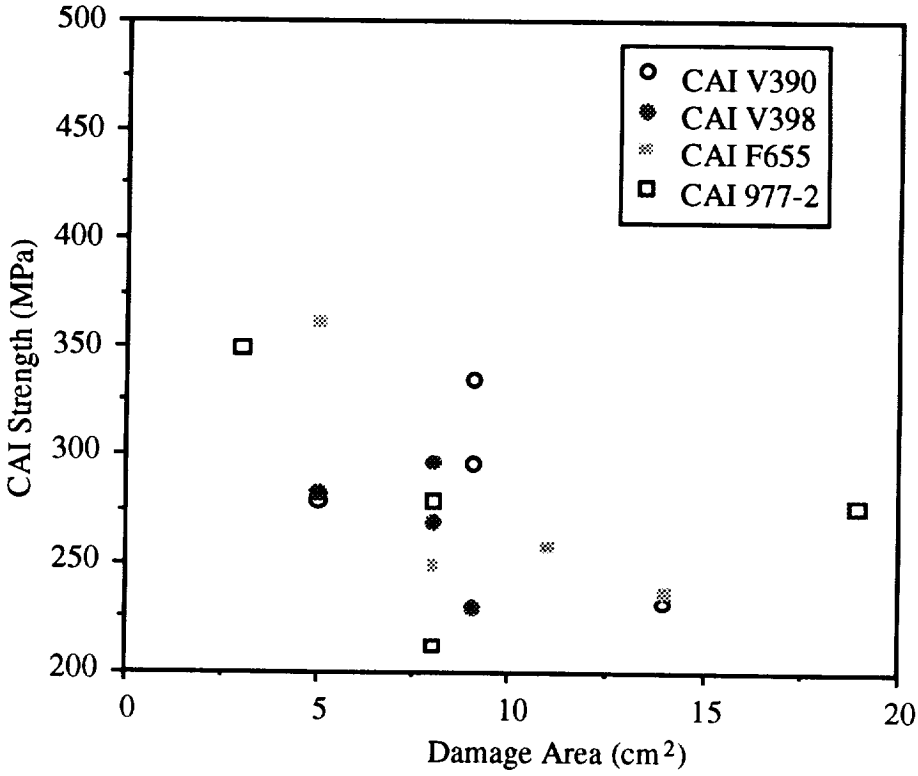

Figure 23. CAI strength versus damage area, 8-ply specimens.

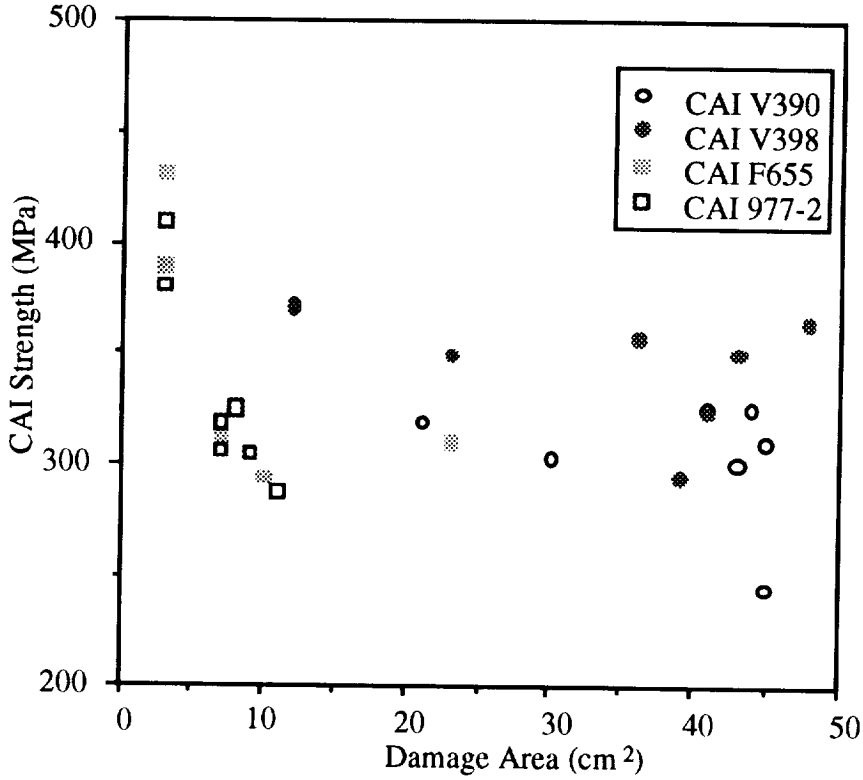

Figure 24. CAI strength versus damage area, 16-ply specimens.

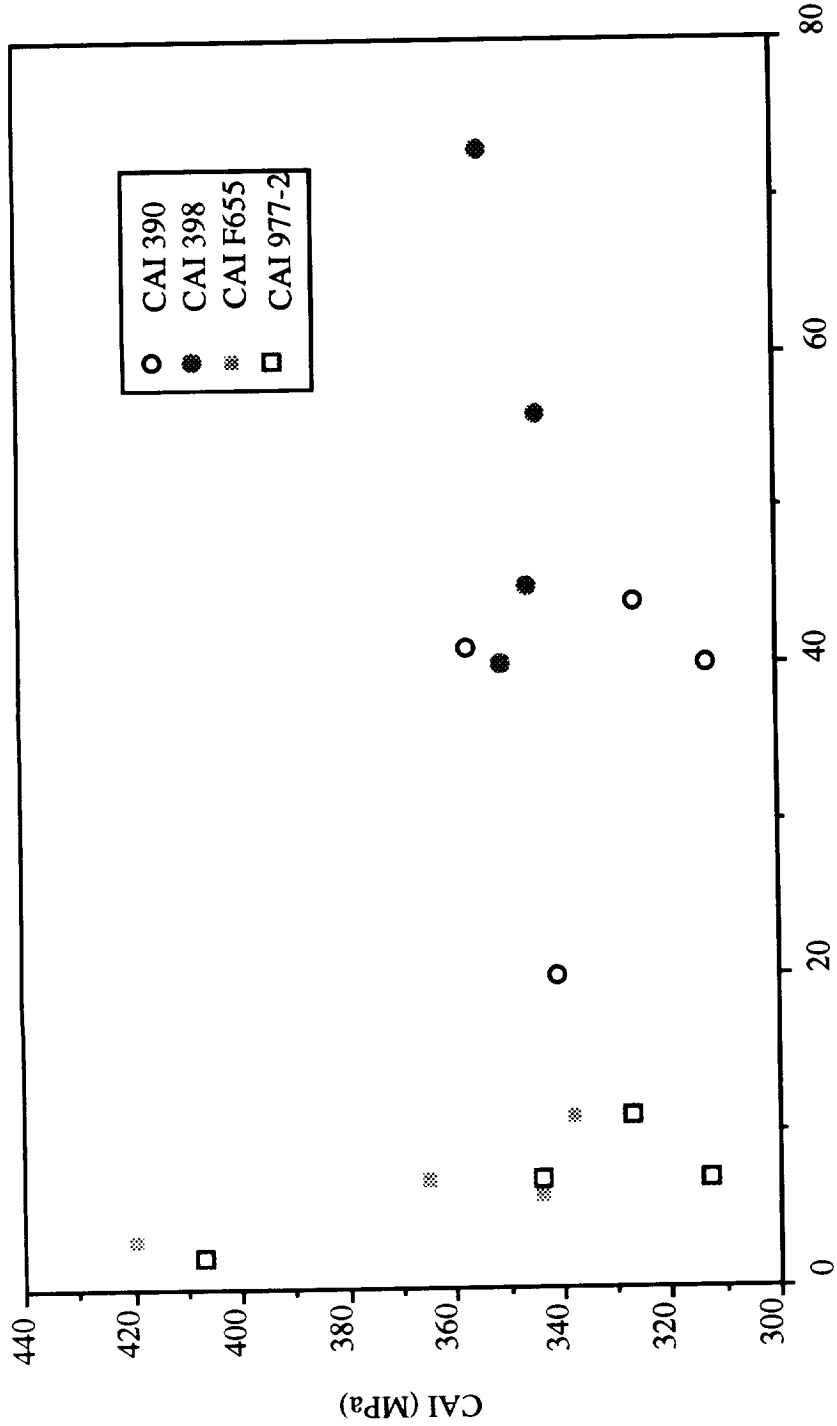

Figure 25. CAI strength versus damage area, 24-ply specimens.

REFERENCES

1. Klein, A.J.: "High-Temperature Imides." Advanced Composites, July/August, 1988.

2. Young, P.R,. and Chang, A.C.: "FTIR Characterization of Thermally Cycled PMR-15 Composites." Proceedings of the 33rd Int. SAMPE Sym., 1988, pp. 538–550.

3. Johnson, S.R. and Sun, C.T., "Impact Damage in Polyimide Composite Laminates." Proceedings of the 33rd Int. Sampe Sym., 1988, pp. 1200–1209.

4. Stenzenberger, H.D., Herzog, M., Konig, P., Rome, W., and Breitigan,W.: "Bismaleimide Resins: Past, Present, Future." Proc. 34th Int. SAMPE Sym., 1989, pp. 1877–1888.

5. Konarski, M.M.: "V-391, A Novel Composite Matrix With the Temperature Performance of BMI's and the Toughness of Thermoplastics." Proceedings of the 34th Int. SAMPE Sym., 1989, pp. 505–513.

6. Stenzenberger, H.D., Konis, P., Romer, W., Herzog, M., and Breitigan, W.V.: "BMI/(Bis-(Allylphenoxyphthalimide)—copolymers: A New Family of Resins for Advanced Composites with Improved Thermal Oxidative Stability." Proceedings of the 36th Int. SAMPE Sym., 1991, pp. 1232–1241.

7. Blair, M.T., Steiner, P.A., and Willis, E.N.: "The Toughening Effects of PBI in a BMI Matrix Resin." Proceedings of the 33rd Int. SAMPE Sym., 1988, pp. 524–537.

8. Liao, Y.T., Lee, K.C., Lin, C.J., and Liu,W.L.: "Interface Properties of High Temperature Polymer Composite Systems." Proceedings of the 35th Int. SAMPE Sym., 1990, pp. 72–81.

9. Almen, G.R., Byrens, R.M., MacKenzie, P.D., Maskell, R.K., McGrail, P.T., and Sefton, M.S., "977—A Family of New Toughened Epoxy Matrices." Proceedings of the 34th Int. SAMPE Sym., 1989, pp. 259–270.

10. Almen, G.R., MacKenzie, P.D., Malhotra, V., and Maskell, R .K.: "977: Characterization of a Family of New Toughened Epoxy Resins." Proceedings of the 35th Int. SAMPE Sym., 1990, pp. 419–431.

11. Dost, E.F., Avery, W.B., Ilcewicz, L.B., Grande, D.H., and Coxon, B.R.: "Impact Damage Resistance of Composite Fuselage Structure, Part I." Proceedings of the Ninth DoD/NASA/FAA Conference on Fibrous Composites in Structural Design, 1991, pp. 1037–1069.

12. Nettles, A.T. and Hodge, A.J.: "Compression-After-Impact Testing of Thin Composite Materials." Proceedings of the 23rd Int. SAMPE Sym., 1991, pp. 177–183.

13. Nettles, A.T.: "A Low Cost Method of Testing Compression-After-Impact Strength of Composite Laminates." NASA CP 3136, vol. 2, 1991, pp. 22–31.

14. Greenhalgh, E.S.: "Delamination Growth in Carbon-Fiber Composite Structures." Composite Structures, vol. 23, 1993, pp. 165–175.

15. Whitcomb, J.D.: "Instability-Related Delamination Growth of Embedded and Edge Delaminations." Ph.D. Dissertation, Virginia Polytechnic Institute and State University, 1988.

16. Nicholls, D.T. and Gallagher, J.P.: "Determination of G_{IC} in Angle Ply Composites." Journal of Reinforced Plastics and Composites, vol. 2, 1983, pp. 2–17.

APPENDIX

C-SCANS AND ASSOCIATED MAXIMUM LOAD OF IMPACT, DAMAGE AREA, VISUAL DAMAGE AND CAI STRENGTH DATA

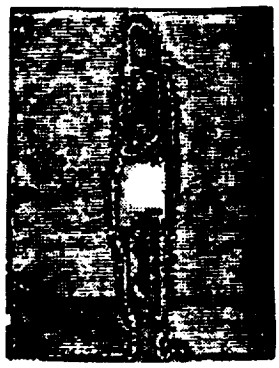

IM7/977-2 #6
8 plies
12 Joules
.5 inch tup
634 lb max
2.9 sq. in.
Hole
40,087 PSI

IM7/977-2 # 8
8 plies
4 Joules
.5 inch tup
552 lb max
.5 sq. in.
Small Split;
Small Dent
50,712 PSI

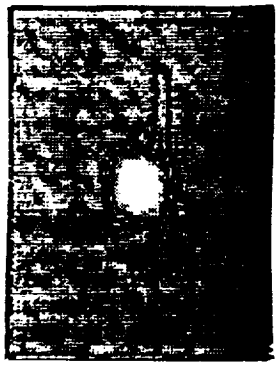

IM7/977-2 # 10
8 plies
8 Joules
.75 inch tup
829 lb max
1.2 sq. in.
Split;
Dent
30,749 PSI

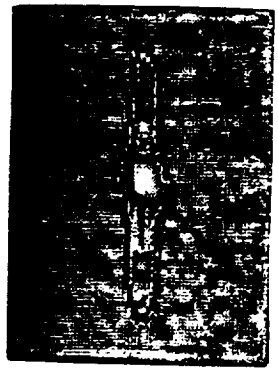

IM7/977-2 #12
8 plies
8 Joules
.25 inch tup
476 lb
1.3 sq. in.
Hole
40,381 PSI

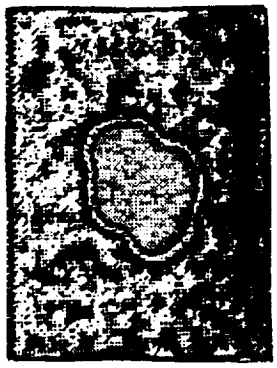

IM7/977-2 #5
24 plies
12 Joules
.5 inch tup
1376 lb max
1.7 sq. in.
Small Split
47,483 PSI

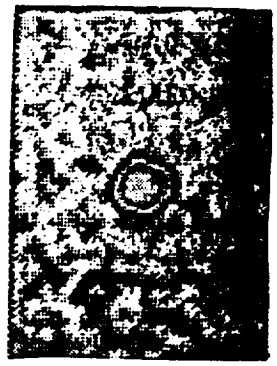

IM7/977-2 #7
24 plies
4 Joules
.5 inch tup
729 lb max
.3 sq. in.
Small Split
59,000 PSI

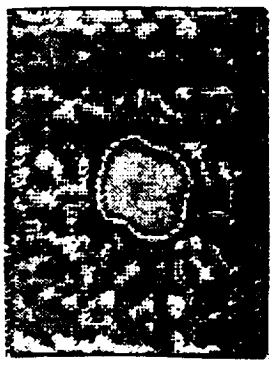

IM7/977-2 #9
24 plies
8 Joules
.75 inch tup
1034 lb max
1.1 sq. in.
No Visible
45,470 PSI

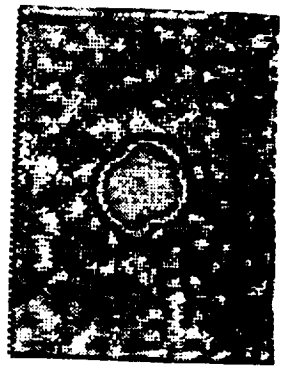

IM7/977-2 # 11
24 plies
8 Joules
.25 inch tup
1032 lb max
1.1 sq. in.
Dent;
Small Split
49,889 PSI

IM7/977-2 # 1
16 plies
12 Joules
.75 inch tup
1201 lb max
1.4 sq. in.
Small Split
44,059 PSI

IM7/977-2 #2
16 plies
12 Joules
.25 inch tup
1040 lb
1.7 sq. in.
Puncture;
Severe Split
41,584 PSI

IM7/977-2 #3
16 plies
4 Joules
.75 inch tup
597 lb max
.5 sq. in.
No Visible
59,488 PSI

IM7/977-2 #4
16 plies
4 Joules
.25 inch tup
600 lb max
.5 sq. in.
Feel Split;
Feel Dent
55,116 PSI

IM7/977-2 #13
16 plies
8 Joules
.8 inch tup
963 lb max
1.1 sq. in.
Minor Split;
Small Dent
46,358 PSI

IM7/977-2 #14
16 plies
8 Joules
.5 inch tup
964 lb max
1.1 sq. in.
Minor Split;
Small Dent
44,463 PSI

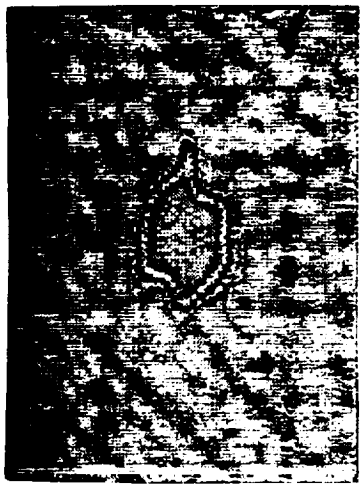

IM7/977-2 #15
16 plies
8 Joules
.5 inch tup
966 lb max
1.2 sq. in.
Minor Split;
Small Dent
47,103 PSI

IM7/F655 #6
8 plies
12 Joules
.5 inch tup
520 lb max
2.1 sq. in.
Hole
34,214 PSI

IM7/F655 # 8
8 plies
4 Joules
.4 inch tup
558 lb max
.8 sq. in.
Small Split;
Small Dent
52,483 PSI

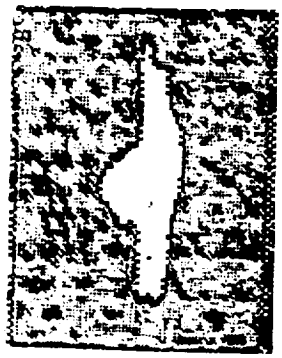

IM7/F655 # 10
8 plies
8 Joules
.75 inch tup
915 lb max
1.7 sq. in.
Split;
Dent
37,525 PSI

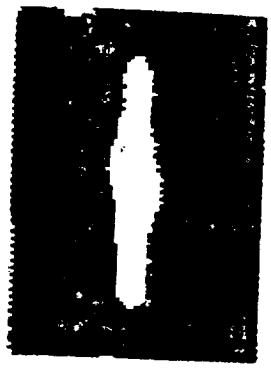

IM7/F655 #12
8 plies
8 Joules
.25 inch tup
429 lb
1.3 sq. in.
Hole
36,087 PSI

IM7/F655 #5
24 plies
12 Joules
.5 inch tup
1403 lb max
1.7 sq. in.
Small Split
49,012 PSI

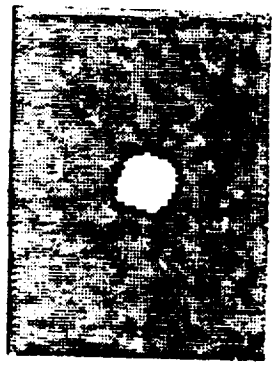

IM7/F655 #7
24 plies
4 Joules
.5 inch tup
805 lb max
.4 sq. in.
Small Split
61,000 PSI

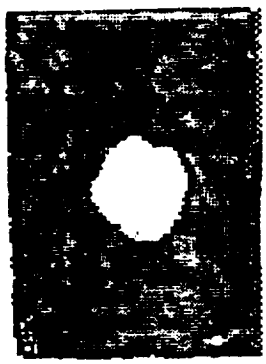

IM7/F655 #9
24 plies
8 Joules
.75 inch tup
854 lb max
1.1 sq. in.
No Visible
53,015 PSI

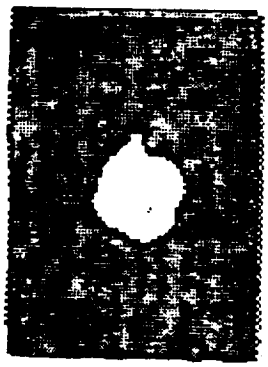

IM7/F655 # 11
24 plies
8 Joules
.25 inch tup
819 lb max
.9 sq. in.
Dent;
Small Split
49,948 PSI

IM7/F655 # 1
16 plies
12 Joules
.75 inch tup
1227 lb max
3.6 sq. in.
Small Split
45,036 PSI

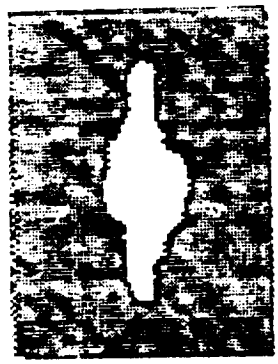

IM7/F655 #2
16 plies
12 Joules
.25 inch tup
662 lb
1.5 sq. in.
Puncture;
Severe Split
42,632 PSI

IM7/F655 #3
16 plies
4 Joules
.75 inch tup
634 lb max
.5 sq. in.
No Visible
62,639 PSI

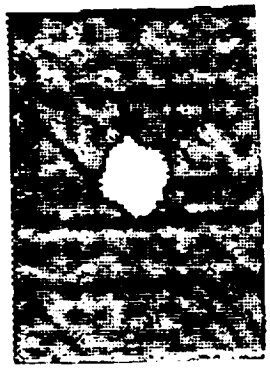

IM7/F655 #4
16 plies
4 Joules
.25 inch tup
527 lb max
.5 sq. in.
Feel Split;
Feel Dent
56,467 PSI

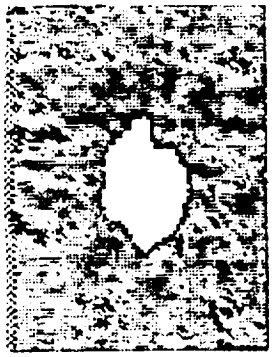

IM7/F655 #13
16 plies
8 Joules
.5 inch tup
991 lb max
1.1 sq. in.
Minor Split;
Small Dent
44,367 PSI

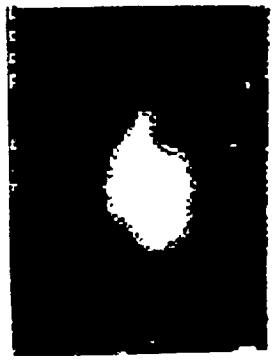

IM7/F655 #14
16 plies
8 Joules
.5 inch tup
982 lb max
1.2 sq. in.
Minor Split;
Small Dent
46,940 PSI

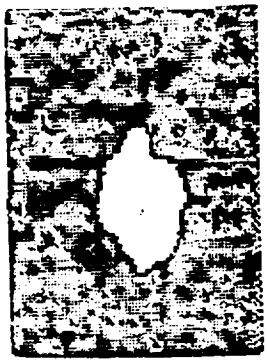

IM7/F655 #15
16 plies
8 Joules
.5 inch tup
974 lb max
1.1 sq. in.
Minor Split;
Small Dent
45,181 PSI

IM7/V398 #6
8 plies
12 Joules
.5 inch tup
649 lb max
1.4 sq. in.
Hole
33,273 PSI

IM7/V398 # 8
8 plies
4 Joules
.5 inch tup
587 lb max
.8 sq. in.
Small Split
49,985 PSI

IM7/V398 # 10
8 plies
8 Joules
.75 inch tup
943 lb max
1.3 sq. in.
Split
43,000 PSI

IM7/V398 #12
8 plies
8 Joules
.25 inch tup
502 lb
1.2 sq. in.
Hole
39,064 PSI

IM7/V398 #5
24 plies
12 Joules
.5 inch tup
1215 lb max
6.2 sq. in.
Feel Split
50,608 PSI

IM7/V398 #7
24 plies
4 Joules
.5 inch tup
676 lb max
6.9 sq. in.
Small Slit
50,228 PSI

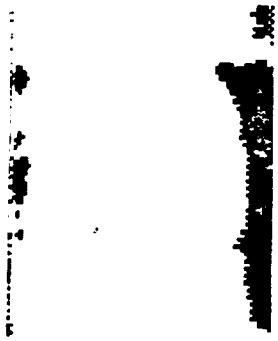

IM7/V398 #9
24 plies
8 Joules
.75 inch tup
902 lb max
11.3 sq. in.
Feel Split
51,383 PSI

IM7/V398 # 11
24 plies
8 Joules
.25 inch tup
844 lb max
8.7 sq. in.
No Visible
49,985 PSI

IM7/V398 # 1
16 plies
12 Joules
.75 inch tup
1328 lb max
5.6 sq. in.
Small Split
51,877 PSI

IM7/V398 #2
16 plies
12 Joules
.25 inch tup
667 lb
6.0 sq. in.
Puncture
42,845 PSI

IM7/V398 #3
16 plies
4 Joules
.75 inch tup
572 lb max
3.5 sq. in.
No Visible
50,608 PSI

IM7/V398 #4
16 plies
4 Joules
.25 inch tup
593 lb max
1.8 sq. in.
Small Split
53,873 PSI

IM7/V398 #13
16 plies
8 Joules
.5 inch tup
906 lb max
6.6 sq. in.
Small Split
50,789 PSI

IM7/V398 #14
16 plies
8 Joules
.5 inch tup
921 lb max
7.5 sq. in.
Minor Split
52,780 PSI

IM7/V398 #15
16 plies
8 Joules
.5 inch tup
901 lb max
6.3 sq. in.
Minor Split
46,913 PSI

IM7/V390 #6
8 plies
12 Joules
.5 inch tup
569 lb max
2.1 sq. in.
Hole
33,504 PSI

IM7/V390 # 8
8 plies
4 Joules
.5 inch tup
585 lb max
.8 sq. in.
Small Split
40,351 PSI

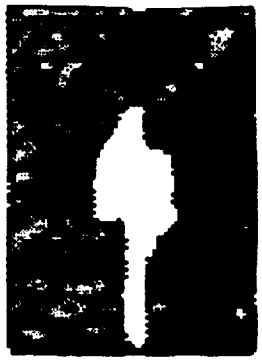

IM7/V390 # 10
8 plies
8 Joules
.75 inch tup
950 lb max
1.4 sq. in.
Split
42,850 PSI

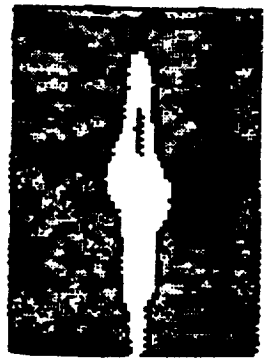

IM7/V390 #12
8 plies
8 Joules
.25 inch tup
478 lb
1.4 sq. in.
Hole
48,495 PSI

IM7/V390 #5
24 plies
12 Joules
.5 inch tup
1290 lb max
6.8 sq. in.
Small Split
47,273 PSI

IM7/V390 #7
24 plies
4 Joules
.5 inch tup
629 lb max
3.1 sq. in.
Felt Dent
49,515 PSI

IM7/V390 #9
24 plies
8 Joules
.75 inch tup
814 lb max
6.3 sq. in.
Small Dent
51,800 PSI

IM7/V390 # 11
24 plies
8 Joules
.25 inch tup
817 lb max
6.2 sq. in.
Small Dent;
Small Split
45,455 PSI

IM7/V390 # 1
16 plies
12 Joules
.75 inch tup
1322 lb max
7.0 sq. in.
Small Split
45,045 PSI

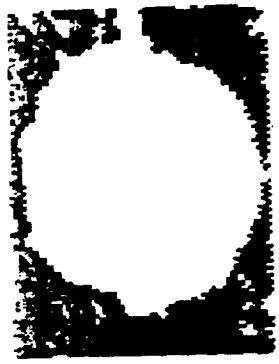

IM7/V390 #2
16 plies
12 Joules
.25 inch tup
753 lb
6.9 sq. in.
Puncture
35,556 PSI

IM7/V390 #3
16 plies
4 Joules
.75 inch tup
556 lb max
4.7 sq. in.
No Visible
44,000 PSI

IM7/V390 #4
16 plies
4 Joules
.25 inch tup
542 lb max
3.2 sq. in.
Feel Split
46,578 PSI

IM7/V390 #13
16 plies
8 Joules
.5 inch tup
937 lb max
6.6 sq. in.
Feel Split
43,733 PSI

IM7/V390 #14
16 plies
8 Joules
.5 inch tup
934 lb max
6.8 sq. in.
Minor Split:
Small Dent
47,289 PSI

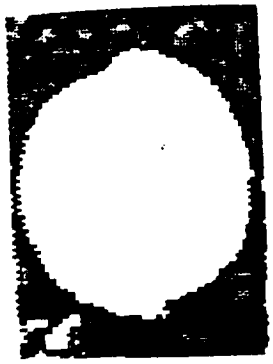

IM7/V390 #15
16 plies
8 Joules
.5 inch tup
937 lb max
6.3 sq. in.
Minor Split:
Small Dent
47,200 PSI

REPORT DOCUMENTATION PAGE

Form Approved
OMB No. 0704-0188

1. AGENCY USE ONLY (Leave blank)	2. REPORT DATE	3. REPORT TYPE AND DATES COVERED
	September 1994	Technical Paper

4. TITLE AND SUBTITLE
Damage Tolerance of Candidate Thermoset Composites for Use on Single Stage to Orbit Vehicles

5. FUNDING NUMBERS

6. AUTHOR(S)
A.T. Nettles, D. Lance, and A. Hodge

7. PERFORMING ORGANIZATION NAME(S) AND ADDRESS(ES)
George C. Marshall Space Flight Center
Marshall Space Flight Center, Alabama 35812

8. PERFORMING ORGANIZATION REPORT NUMBER
M-758

9. SPONSORING/MONITORING AGENCY NAME(S) AND ADDRESS(ES)
National Aeronautics and Space Administration
Washington, DC 20546

10. SPONSORING/MONITORING AGENCY REPORT NUMBER
NASA TP-3506

11. SUPPLEMENTARY NOTES
Prepared by Materials and Processes Laboratory, Science and Engineering Directorate.

12a. DISTRIBUTION/AVAILABILITY STATEMENT
Subject Category: 24
Unclassified—Unlimited

12b. DISTRIBUTION CODE

13. ABSTRACT (Maximum 200 words)

Four fiber/resin systems were compared for resistance to damage and damage tolerance. One toughened epoxy and three toughened bismaleimide (BMI) resins were used, all with IM7 carbon fiber reinforcement. A statistical design of experiments technique was used to evaluate the effects of impact energy, specimen thickness, and tup diameter on the damage area as computed by C-scans, and residual compression-after-impact (CAI) strength. Results showed that two of the BMI systems sustained relatively large damage zones yet had an excellent retention of CAI strength.

14. SUBJECT TERMS
composite materials, damage tolerance

15. NUMBER OF PAGES
49

16. PRICE CODE
A03

17. SECURITY CLASSIFICATION OF REPORT	18. SECURITY CLASSIFICATION OF THIS PAGE	19. SECURITY CLASSIFICATION OF ABSTRACT	20. LIMITATION OF ABSTRACT
Unclassified	Unclassified	Unclassified	Unlimited